

Maternal Ezh1/2 deficiency in oocyte delays H3K27me2/3 restoration and impairs epiblast development responsible for embryonic sub-lethality in mouse

Yinan Zhao^{1,*}, Dandan Bai^{2,*}, You Wu^{2,*}, Dan Zhang¹, Mengying Liu¹, Yingpu Tian¹, Jinhua Lu³, Haibin Wang^{3,†}, Shaorong Gao^{2,†} and Zhongxian Lu^{1,3,‡}

ABSTRACT

How maternal Ezh1 and Ezh2 function in H3K27 methylation *in vivo* in pre-implantation embryos and during embryonic development is not clear. Here, we have deleted Ezh1 and Ezh2 alone or simultaneously from mouse oocytes. H3K27me3 was absent in oocytes without Ezh2 alone, while both H3K27me2 and H3K27me3 were absent in Ezh1/Ezh2 (Ezh1/2) double knockout (KO) oocytes. The effects of Ezh1/2 maternal KO were inherited in zygotes and early embryos, in which restoration of H3K27me3 and H3K27me2 was delayed by the loss of Ezh2 alone or of both Ezh1 and Ezh2. However, the ablation of both Ezh1 and Ezh2, but not Ezh1 or Ezh2 alone, led to significantly decreased litter size due to growth retardation post-implantation. Maternal Ezh1/2 deficiency caused compromised H3K27me3 and pluripotent epiblast cells in late blastocysts, followed by defective embryonic development. By using RNA-seq, we examined crucial developmental genes in maternal Ezh1/2 KO embryos and identified 80 putatively imprinted genes. Maternal Ezh1/2-H3K27 methylation is inherited in offspring embryos and has a critical effect on fetal and placental development. Thus, this work sheds light on maternal epigenetic modifications during embryonic development.

KEY WORDS: Ezh1, Ezh2, H3K27me3, Embryonic development

INTRODUCTION

Mammalian embryonic development begins with the formation of a zygote and ends with a fully developed fetus. This complex process is accompanied by a variety of epigenetic modifications (Saitou et al., 2012). Histone modifications are found to play key roles in epigenetic regulation (Canovas and Ross, 2016). Methylations at lysine 4, 9 and 27 on histone H3 act as transcriptional modulators and regulate specific sets of genes involved in embryogenesis, embryonic stem cell (ESC) pluripotency and differentiation,

tissue stem cell maintenance, the establishment and maintenance of genomic imprinting, and tumorigenesis (Jambhekar et al., 2019; Michalak et al., 2019; Yu et al., 2019). Recently, dynamic patterns of H3K4 trimethylation (H3K4me3) and H3K27 trimethylation (H3K27me3), which play crucial roles in maternal X-chromosome inactivation (XCI), zygotic genome activation (ZGA) and developmental genes, have been illustrated in mouse oocytes and pre-implantation embryos (Inoue et al., 2018; Liu et al., 2016; Zhang et al., 2016). Histone modifications are germline modifications that are inherited or re-established during early embryogenesis (Liu et al., 2016; Zhang et al., 2016; Zheng et al., 2016). However, the regulation and underlying mechanisms of maternal histone modifications in embryonic development need to be fully explored.

PRC2 is a histone methyltransferase (HMT) complex that produces cell type-specific H3K27 mono- (H3K27me1), di- (H3K27me2) and trimethylation (H3K27me3) patterns (Bracken et al., 2006; Ferrari et al., 2014). H3K27me3 is a well-known repressive histone modification that ultimately causes transcriptional silencing (Cao et al., 2002). In mammals, the core subunits of the PRC2 complex include enhancer of zeste homolog 1 or 2 (Ezh1 or Ezh2), embryonic ectoderm development (Eed), suppressor of zeste 12 (Suz12) and retinoblastoma-binding protein 4/7 (Rbpb4/7) (Yan et al., 2019). Ezh1 and Ezh2 are the catalytic subunits of the PRC2 complex (Margueron and Reinberg, 2011). In *Drosophila*, deletion of Enhancer of zeste [E(z)] during oogenesis causes embryonic lethality, even though H3K27me3 is re-established in late zygotes (Zenk et al., 2017), indicating that H3K27me3 establishment during early embryogenesis requires maternal PRC2. However, the effects of maternal PRC2 on mammalian embryonic development remain unclear, and related reports are inconsistent. In mice, the oocyte-specific deletion of *Ezh2* by *Zp3-Cre* does not alter litter size but cause growth retardation in the progeny (Erhardt et al., 2003). Maternal *Eed* knockout by *Gdf9-Cre* shows loss of H3K27me3 imprinting and growth arrest post-implantation (Inoue et al., 2018). Elimination of *Eed* from growing oocytes by *Zp3-Cre* results in a significant overgrowth phenotype that persists into adult life (Prokopuk et al., 2018). These results indicate that *Ezh2* and *Eed* may have different functions in post-embryonic development (Prokopuk et al., 2018). Collectively, these discoveries suggest that maternal PRC2 core components have a long-term effect on the development of descendants of the mother. However, the exact details of this process remain to be discovered. Recently, a report showed that Ezh2 is required for the establishment of H3K27me3 in mouse zygotes, and Ezh1 could partially safeguard the role of Ezh2 (Meng et al., 2020), indicating that *Ezh1* might compensate for *Ezh2* in specific developmental contexts (Ezhkova et al., 2011; Mochizuki-Kashio et al., 2015). However, how maternal Ezh1 and Ezh2

¹School of Pharmaceutical Sciences, State Key Laboratory of Cellular Stress Biology, Xiamen University, Xiamen, Fujian 361005, China. ²Shanghai Key Laboratory of Signaling and Disease Research, School of Life Sciences and Technology, Tongji University, Shanghai 200092, China. ³Fujian Provincial Key Laboratory of Reproductive Health Research, Medical College of Xiamen University, Xiamen, Fujian 361102, China.

*These authors contributed equally to this work

†Authors for correspondence (zhongxian@xmu.edu.cn; gaoshaorong@tongji.edu.cn; haibin.wang@vip.163.com)

Y.Z., 0000-0002-9501-4725; D.Z., 0000-0003-4818-4673; M.L., 0000-0002-5987-1287; J.L., 0000-0002-4164-4238; H.W., 0000-0002-9865-324X; S.G., 0000-0003-1041-3928

comprehensively mediate H3K27 methylation in pre-implantation embryos *in vivo* is unknown.

To investigate this issue, we used maternal *Ezh1/2* knockout mice to gain insights into the dynamic patterns of H3K27 methylation during the pre-implantation period and reveal their regulatory effects on embryonic development. The results demonstrate that maternal *Ezh1* and *Ezh2* are required for the establishment of H3K27me2/3 in pre-implantation embryos *in vivo* and play crucial roles in embryonic development in mouse.

RESULTS

Recovery of H3K27me3 and H3K27me2 is delayed in early maternal knockout embryos

To reveal the maternal PRC2-mediated histone modifications and their long-term effects on embryonic development, we used an *Ezh1*-null mouse line and *Gdf9*-Cre transgenic mice to construct transgenic mouse models with *Ezh1* and *Ezh2* deletion in growing oocytes. Here, we have established two pairs of mouse lines: sCtrl (single control, no *Ezh1* and *Ezh2* KO) and sKO (single knockout of *Ezh2* in oocytes via *Gdf9*-Cre) (Fig. S1A); and dCtrl (double control, that is, *Ezh1* knockout) and dKO (double knockout of both *Ezh1* and *Ezh2* in oocytes) (Fig. S2A). In sKO mice, the mRNA and protein levels of *Ezh2* in the oocytes were undetectable (Fig. S1B and C), whereas the expression of the other PRC2 core components, *Ezh1*, *Eed* and *Suz12*, was not affected (Fig. S1B). In dKO mice, the *Ezh1* and *Ezh2* genes were deleted, whereas the mRNA levels of *Eed* and *Suz12* were not affected (Fig. S2B and C). These observations showed that *Ezh1*

and *Ezh2* in oocytes were successfully deleted in oocytes in these mice.

The PRC2 complex is responsible for methylation of H3K27 through its enzymatic subunits *Ezh1* and *Ezh2* (Schuettengruber and Cavalli, 2009; Simon and Kingston, 2009). We therefore checked the H3K27me2/3 modifications in oocytes by immunohistochemistry (IHC) and immunofluorescence (IF). H3K27me3 was absent in oocytes from secondary follicles and MII oocytes from both sKO (Fig. S1D,E) and dKO mice (Fig. S2D-F). However, H3K27me2 was absent only in the MII oocytes of dKO mice, but not in those of sKO or dCtrl mice (Fig. S2F). These results suggest that *Ezh2* is indispensable for H3K27me3 modification, where *Ezh1* and *Ezh2* can both facilitate H3K27me2 modification in oocytes.

We then examined the H3K27 methylation patterns at different stages of early embryos. Embryos from sCtrl, sKO, dCtrl and dKO females mated with wild-type males are hereafter referred to as sF (no *Ezh1* and *Ezh2* KO)/+, sKO(single *EZH2* KO)/+, dF(single *EZH1* KO)/+ and dKO (*Ezh1* and *Ezh2* KO)/+ (with F representing flox), respectively. H3K27me3 staining was strong in the female pronucleus (PN) but relatively weak in the paternal PN in sF/+ late zygotes (Fig. 1A). H3K27me3 was clearly detected in sF/+ embryos from the late two-cell stage to the early blastocyst stage, whereas it was not restored until the late blastocyst stage in the sKO/+ groups (Fig. 1A and Fig. S3A), suggesting that the modification of H3K27me3 in pre-implantation embryos is dependent on maternal *Ezh2*. Enhanced H3K27me3 staining in the inner cell mass (ICM) appeared at the sKO/+ late blastocyst stage, along with dot staining in the trophectoderm (TE) in some embryos, which was comparable

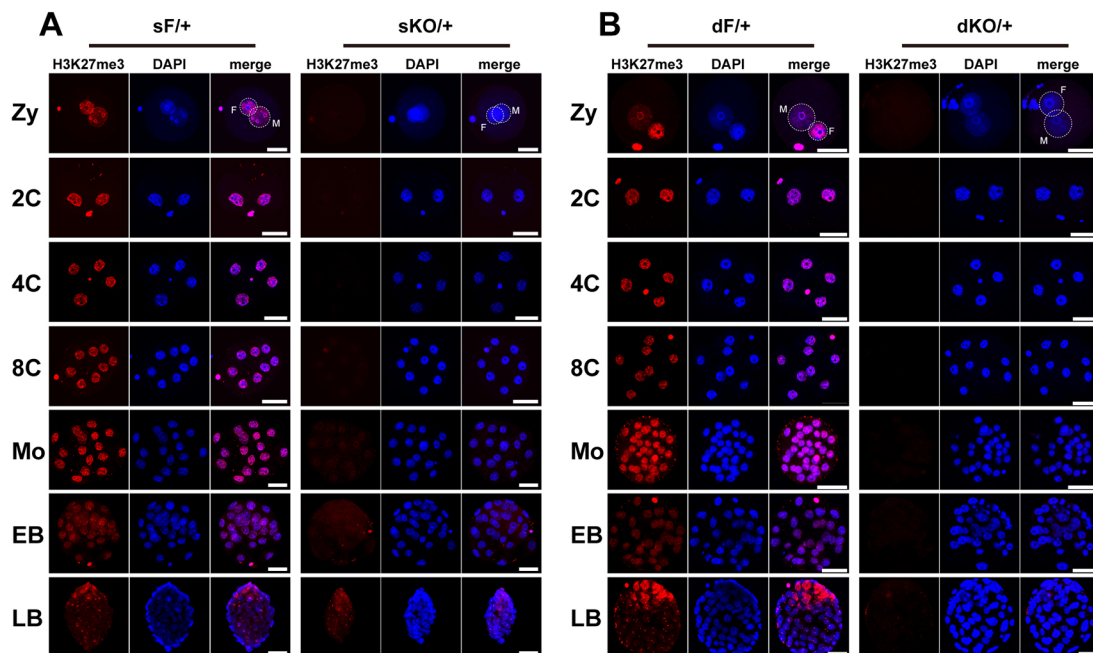


Fig. 1. Delayed recovery of H3K27me3 modification in pre-implantation stage of sKO/+ and dKO/+ embryos. (A) H3K27me3 patterns in sF/+ and sKO/+ embryos. In late zygotes, H3K27me3 was absent in both the male and female pronucleus (PN) of sKO/+. H3K27me3 was not detectable until late blastocysts in sKO/+ embryos. The number of zygotes examined: sF/+, *n*=22; sKO/+, *n*=21. Number of two-cell embryos examined: sF/+, *n*=21; sKO/+, *n*=25. Number of four-cell embryos examined: sF/+, *n*=26; sKO/+, *n*=12. Number of eight-cell embryos examined: sF/+, *n*=12; sKO/+, *n*=16. Number of morula stage embryos examined: sF/+, *n*=9; sKO/+, *n*=12. Number of early blastocyst stage embryos examined: sF/+, *n*=9; sKO/+, *n*=18. Number of late blastocyst stage embryos examined: sF/+, *n*=9; sKO/+, *n*=13. Scale bars: 50 μ m. (B) H3K27me3 patterns in dF/+ and dKO/+ embryos. H3K27me3 was not detectable even in dKO/+ late blastocysts. Number of zygotes examined: dF/+, *n*=19; dKO/+, *n*=14. Number of two-cell embryos examined: dF/+, *n*=25; dKO/+, *n*=18. Number of four-cell embryos examined: dF/+, *n*=20; dKO/+, *n*=17. Number of eight-cell embryos examined: dF/+, *n*=19; dKO/+, *n*=14. Morula: dF/+, *n*=31; dKO/+, *n*=38. Number of early blastocyst stage embryos examined: dF/+, *n*=13; dKO/+, *n*=11. Number of late blastocyst stage embryos examined: dF/+, *n*=4; dKO/+, *n*=11. Scale bars: 50 μ m. Zy, zygote (PN4-PN5); 2C, two-cell embryo; 4C, four-cell embryo; 8C, eight-cell embryo; Mo, morula; EB, early blastocyst; LB, late blastocyst; M, male pronucleus; F, female pronucleus.

with that in sF/+ embryos (Fig. 1A). In addition, H3K27me3 staining was still faint in late blastocysts of dKO/+ embryos (Fig. 1B, right images and Fig. S3B), indicating that maternal *Ezh1/2* have a long-lasting effect on H3K27me3 modification in early embryos.

During normal embryonic development, H3K27me2 and H3K27me3 have similar expression patterns. In sKO/+ embryos, the H3K27me2 in female PN was very weak in contrast to that in sF/+, and that in the paternal PN was almost undetectable (Fig. 2A, right images). Furthermore, H3K27me2 in sKO/+ embryos was detected at the two-cell stage and was comparable with that in sF/+ embryos at the four-cell and morula stages, followed by decreased intensity at the eight-cell and blastocyst stages (Fig. 2A and Fig. S3C). However, H3K27me2 staining in dKO/+ embryos was absent from the zygote to the eight-cell stage, faint from the morulae to the early blastocysts and then fully recovered at the late blastocyst stage (Fig. 2B, right images; Fig. S3D), indicating that maternal *Ezh1* in conjunction with *Ezh2* plays an important role in H3K27me2 modification.

Together, these observations demonstrate that H3K27 methylation activated by maternal PRC2 is dominant in pre-implantation embryos and that maternal *Ezh2* is required for H3K27me3 modification, while maternal *Ezh1* assists in H3K27me2 modification.

Double knockout of *Ezh1* and *Ezh2* in oocytes results in female subfertility

Next, we investigated the reproductive performance of the KO mice. KO females were mated with wild-type males. The cumulative

number of pups, number of pups per litter and the number of litters per mouse were analyzed. The results showed that sKO females had normal fertility (Fig. 3A–C). Although the cumulative number of pups produced from dKO females was obviously lower than that of dCtrl females (Fig. 3D), the average litter size of dKO females (2.69 ± 1.35) was significantly smaller than that of dCtrl females (7.10 ± 2.13) (Fig. 3E). The number of litters per mouse was also greatly decreased in dKO females (Fig. 3F). These data suggest that the loss of both *Ezh1* and *Ezh2* in oocytes impaired female fertility in mice.

Maternal *Ezh1/2* knockout embryos develop abnormally after implantation

As histone modifications are broadly reprogrammed during gametogenesis (Matsui and Mochizuki, 2014; Zheng et al., 2016), we first examined ovary development and ovulation to reveal the cause of the subfertility. In dKO females, ovarian morphology was not affected and follicles developed normally (Fig. S4A). The average number of ovulated oocytes in the dKO groups was also similar to that of dCtrl mice (Fig. S4B,C). Moreover, there was no difference in the number of implantation sites on day 5 of pregnancy between dKO and dCtrl females (Fig. S4D,E), indicating that pre-implantation development and embryo implantation were normal. These results suggest that the observed decrease in fertility is not due to defects in oogenesis and implantation.

We then focused on post-implantation embryos and isolated embryos at E10.5, when the mouse embryo is undergoing

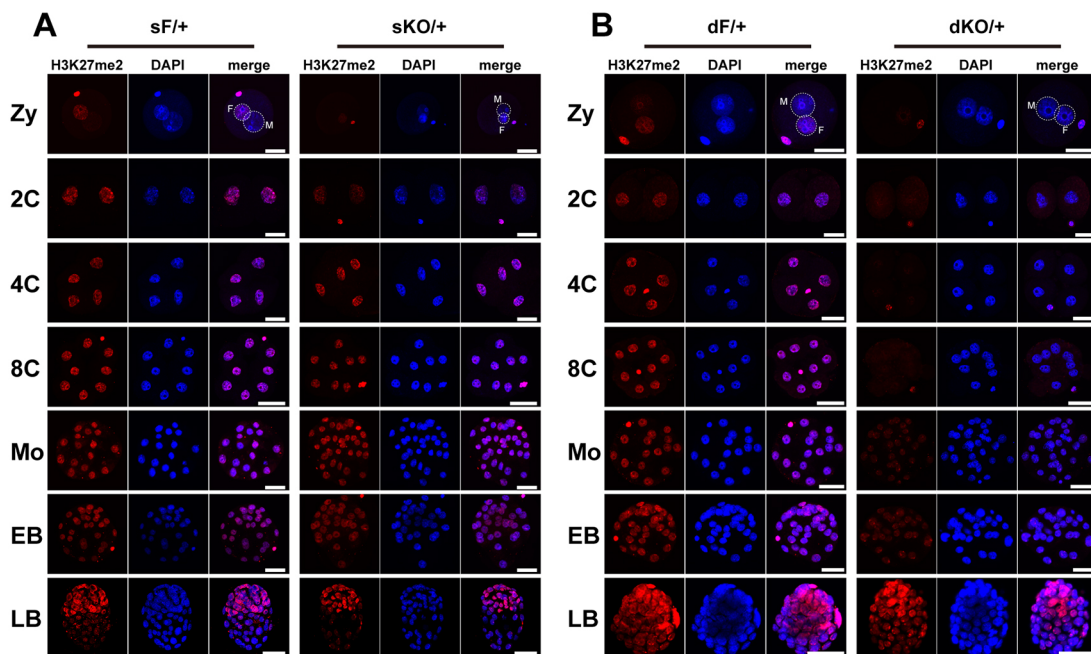


Fig. 2. Delayed recovery of H3K27me2 modification in the pre-implantation stage of sKO/+ and dKO/+ embryos. (A) H3K27me2 patterns in sF/+ and sKO/+ embryos. In sKO/+ late zygotes, H3K27me2 was undetectable in the male PN and faint in the female PN. H3K27me2 was recovered completely in four-cell embryos in sKO/+. Number of zygotes examined: sF/+, $n=21$; sKO/+, $n=20$. Number of two-cell embryos examined: sF/+, $n=38$; sKO/+, $n=19$. Number of four-cell embryos examined: sF/+, $n=30$; sKO/+, $n=13$. Number of eight-cell embryos examined: sF/+, $n=36$; sKO/+, $n=44$. Number of morula stage embryos examined: sF/+, $n=8$; sKO/+, $n=10$. Number of early blastocyst stage embryos examined: sF/+, $n=12$; sKO/+, $n=5$. Number of late blastocyst stage embryos examined: sF/+, $n=13$; sKO/+, $n=5$. Scale bars: 50 μ m. (B) H3K27me2 patterns in dF/+ and dKO/+ embryos. H3K27me2 in dKO/+ embryos was not detectable until the morula stage. Note the isolated signals in morulae and blastocysts. Number of zygotes examined: dF/+, $n=17$; dKO/+, $n=10$. Number of four-cell embryos examined: dF/+, $n=12$; dKO/+, $n=13$. Number of eight-cell embryos examined: dF/+, $n=11$; dKO/+, $n=14$. Number of morula stage embryos examined: dF/+, $n=12$; dKO/+, $n=18$. Number of early blastocyst stage embryos examined: dF/+, $n=12$; dKO/+, $n=5$. Number of late blastocyst stage embryos examined: dF/+, $n=4$; dKO/+, $n=14$. Scale bars: 50 μ m. Zy, zygote (PN4–PN5); 2C, two-cell embryo; 4C, four-cell embryo; 8C, eight-cell embryo; Mo, morula; EB, early blastocyst; LB, late blastocyst; M, male pronucleus; F, female pronucleus.

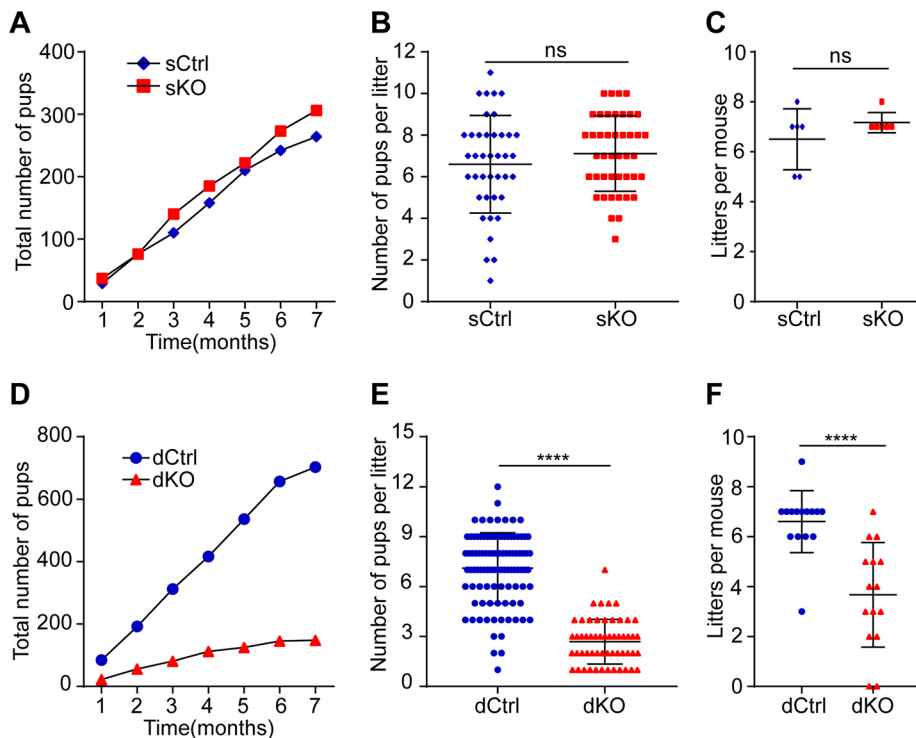


Fig. 3. Double knockout of *Ezh1* and *Ezh2* in oocytes leads to female subfertility.

(A-C) Fertility studies of sCtrl and sKO mice. Number of females: sCtrl, $n=6$; sKO, $n=6$. (A) The cumulative number of pups. (B) The average number of pups per litter. Data are mean \pm s.d. Mann–Whitney test: ns, not significant. (C) The average number of litters per mouse. Data are mean \pm s.d. Mann–Whitney test: ns, not significant. (D-F) Fertility studies of dCtrl and dKO mice. Number of females: dCtrl, $n=15$; dKO, $n=15$. (D) The cumulative number of pups. (E) The average number of pups per litter. Data are mean \pm s.d. Mann–Whitney test: **** $P<0.0001$. (F) The average number of litters per mouse. Data are mean \pm s.d. Mann–Whitney test: **** $P<0.0001$.

organogenesis (Kojima et al., 2014) and the basic structure of the mouse placenta is formed (Rossant and Cross, 2001). Morphologically, the development of the dKO/+ fetus and placenta appeared severely retarded at E10.5 (Fig. 4A). Some embryos (26.83%) had been absorbed and could not be isolated (Fig. 4B). In addition, the decidua weight of dKO females was greatly reduced compared with that of dCtrl females (Fig. 4C), indicating growth restriction. Tissue sections with Hematoxylin and Eosin staining showed that the phenotypes of the dKO/+ embryos at E10.5 could be divided into three categories: type I had a placenta containing a labyrinth (Lab) layer, spongiotrophoblast (Sp) layer (always smaller) and trophoblast giant cells (TGC) (Fig. 4D, left second images); type II had a fetus but had no Lab or Sp (Fig. 4D, right second images); and type III embryos were partially or completely absorbed (Fig. 4D, right first images).

Furthermore, growth retardation of embryos from E5.5–E7.5 was observed in decidual sections (Fig. 4E, E5.5–E7.5). Indeed, analysis of paraffin-embedded sections and tissue dissection under stereoscope showed that the embryos decreased in size beginning at E5.5. Moreover, failure of chorioallantoic attachment and branching was observed in dKO/+ embryos at E9.5, in line with the placental defects observed at E10.5 (Fig. 4E). This demonstrates that growth arrest during the post-implantation phase is responsible for the subfertility in these mice. It is known that chorioallantoic attachment during placental development is dependent on Vcam1, a cell-adhesion molecule that is expressed on the tip of the allantois, and on its ligand integrin $\alpha 4$, which is expressed on the basal surface of the chorion (Rossant and Cross, 2001). However, IHC analysis showed that Vcam1 and integrin $\alpha 4$ were expressed normally in dKO/+ embryos (Fig. 4F,G), indicating that the interactions between Vcam1 and integrin $\alpha 4$ alone are not sufficient for a successful union of the chorion and allantois (Walentin et al., 2016), and other factors may account for the failed chorioallantoic attachment observed in dKO/+ embryos.

Surprisingly, morphological and histological analyses revealed that the placentas of dKO/+ embryos were enlarged in the late stages of pregnancy (Fig. 5A,B), as indicated by the overgrowth of spongiotrophoblasts and increased placental weight at E17.5 (Fig. 5C,F). However, the fetuses were smaller than those in the dF/+ groups (Fig. 5A), with decreased weight and length (Fig. 5D,E).

In summary, the development defects of the embryos fell into three distinct categories. Embryos in the first category ceased development shortly after implantation and could not develop past gastrulation; those in the second category failed to establish placentation and were destined to die; and those in the third category successfully achieved gastrulation and placentation, but were accompanied by a large abnormal placenta and fetal growth restriction.

To determine whether the maternal uterine environment contributed to the observed growth retardation, embryo transfer experiments were pursued. dF/+ and dKO/+ blastocysts were separately transferred to wild-type pseudopregnant recipients. The dKO/+ groups showed a considerably reduced number of term pups (Table S1). This result was consistent with the subfertility of dKO females. Approximately 18% of the dKO/+ blastocysts developed to term pups, much lower than the rate for dF/+ blastocysts (about 48%) (Table S1). This finding indicates that defects in the dKO/+ embryo per se, rather than the maternal uterine environment, contribute to abnormal embryonic development. Above all, these results suggest that maternal *Ezh1/2* deficiency in oocytes disturbs embryonic development and that the loss of maternal *Ezh1/2* has long-lasting consequences for embryogenesis.

Epiblast cells are abnormal in dKO/+ embryos during peri-implantation

To trace the onset and progression of developmental abnormalities, the development of dKO/+ embryos was examined during peri-implantation in mice. Normally, epiblast (EPI) cells differentiated from the inner cell mass (ICM) proliferate rapidly after implantation,

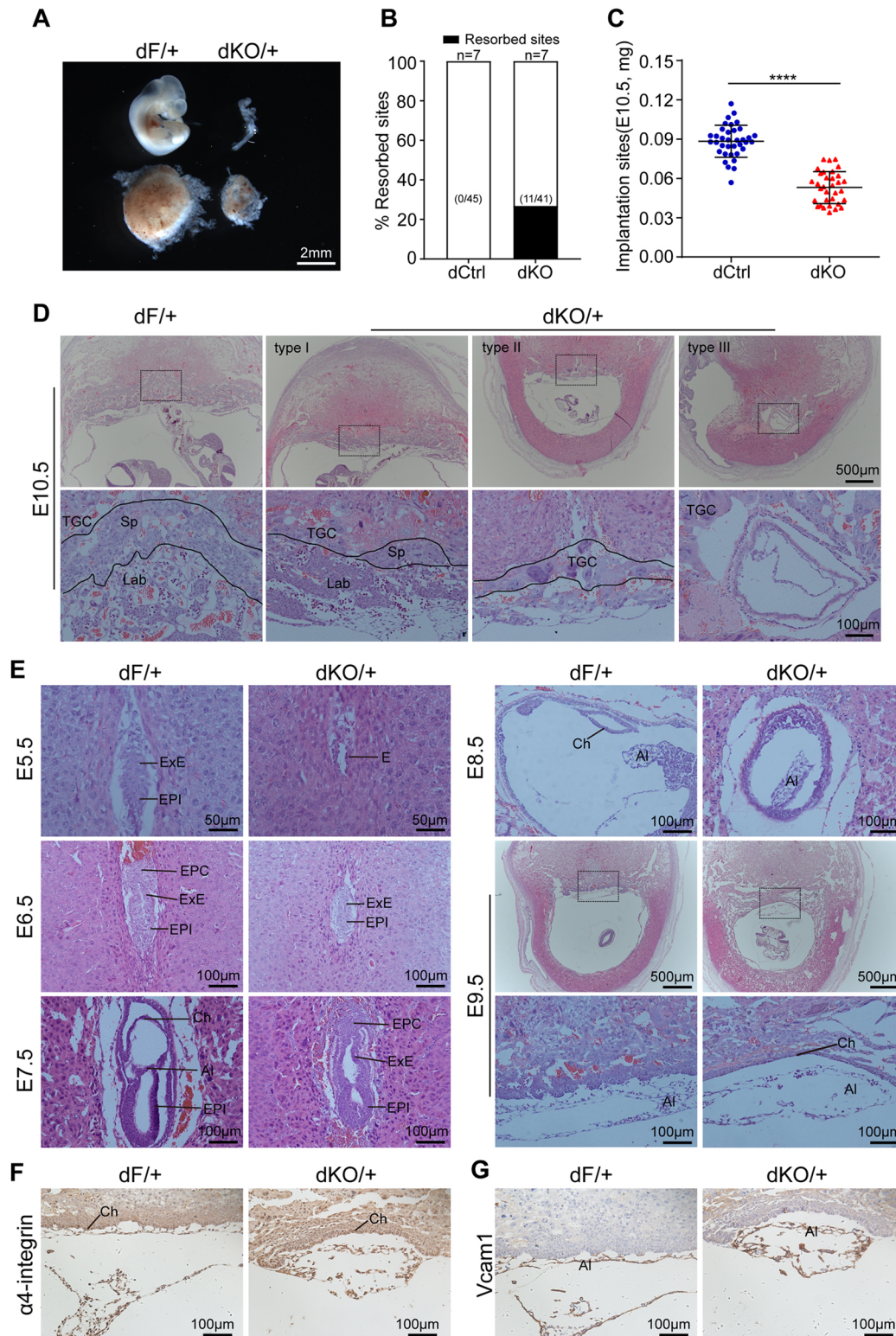


Fig. 4. Double knockout of *Ezh1* and *Ezh2* in oocytes causes growth retardation during the post-implantation phase. (A) Representative images of E10.5 fetuses (top) and placentae (bottom). (B) Ratio of resorption sites at E10.5 in dCtrl and dKO females. Numbers within parentheses indicate the number of resorption sites over the total number of implantation sites. The number of females examined is shown above the bars. (C) The weight of implantation sites at E10.5. Number of implantation sites: dCtrl, $n=36$; dKO, $n=33$. Data are mean \pm s.d. Unpaired t -test: **** $P<0.0001$. (D) Representative images of placentae at E10.5 by Hematoxylin and Eosin (HE) staining. Black rectangles indicate the regions shown at higher magnification in the panels below. (E) Representative images of uterine decidua sections from E5.5 to E9.5 stained using HE. Black rectangles in E9.5 images indicate the regions shown at higher magnification in the panels below. Lines in the bottom left panel at E9.5 indicate progression of labyrinth branching. The image in the bottom right shows failed branching. (F) The expression of integrin $\alpha 4$ in the chorion at E9.5 by immunohistochemical (IHC) staining. (G) Vcam1 expression in allantois at E9.5 by IHC staining. TGC, trophoblast giant cells; Sp, spongiotrophoblast; Lab, labyrinth; ExE, extra-embryonic ectoderm; EPI, epiblast; E, embryo; EPC, ectoplacental cone; Ch, chorion; AI, allantois.

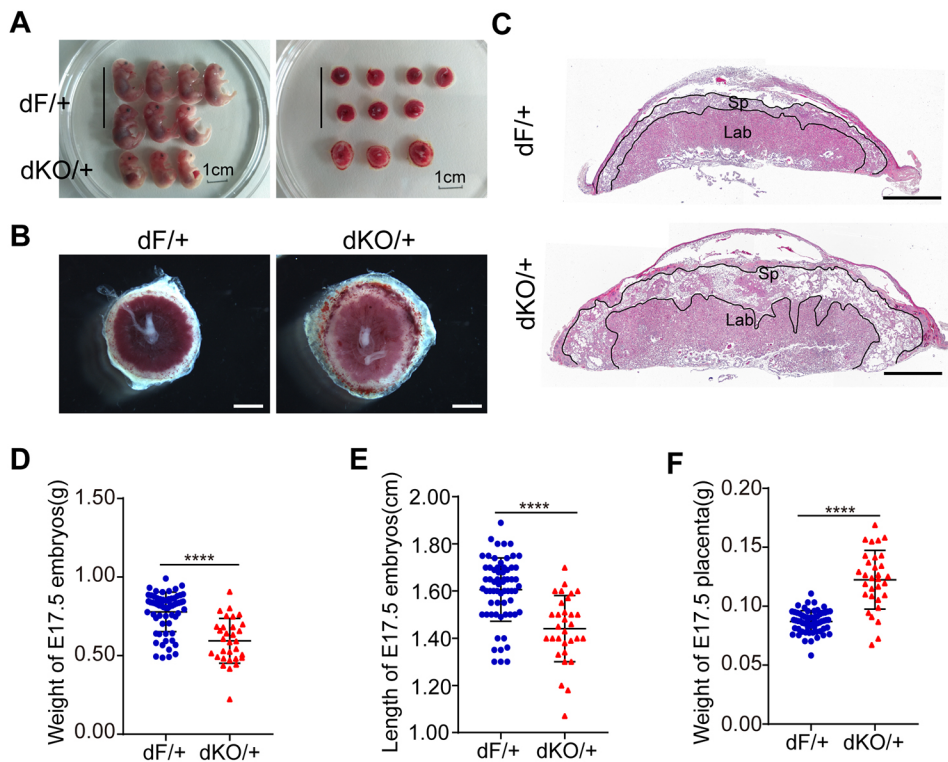


Fig. 5. Placental enlargement in late stage of *dKO/+* embryos. (A) Representative images of E17.5 fetuses and placentae. The top seven embryos are *dF/+*; the bottom three embryos are *dKO/+*. (B) Representative images of E17.5 placentae under the stereoscope. Scale bars: 1 mm. (C) Morphology of E17.5 placentae as evaluated by Hematoxylin and Eosin staining. Sp, spongiotrophoblast; Lab, labyrinth. Scale bars: 1 mm. (D) The weight of fetus at E17.5. Data are mean \pm s.d. Mann-Whitney test: **** P <0.0001. (E) The length of fetus at E17.5. Data are mean \pm s.d. Mann-Whitney test: **** P <0.0001. (F) The weight of placenta at E17.5. Data are mean \pm s.d. Unpaired *t*-test: **** P <0.0001.

and then the embryos form a proamniotic cavity at E5.5, which is a prerequisite for gastrulation (Mole et al., 2020; Tam and Loebel, 2007). However, no discernible epiblast was observed in *dKO/+* embryos at E4.75 (Fig. 6A). Successive sections showed that *dKO/+* embryos had few Oct4⁺ cells at E4.75 (Fig. 6B and Fig. S7A). At E5.5, *dKO/+* embryos had no proamniotic cavity with a reduced EPI area, while *dF/+* embryos showed an obvious proamniotic cavity (Fig. 6C and Fig. S7B). Our careful morphological examinations at different embryonic stages revealed that growth arrest occurs during the peri-implantation period and that EPI/ICM development is defective.

We next sought to determine how the EPI/ICM cells are impaired. In mouse development, the first cell lineage decision occurs before implantation (around at E3.0~3.5) and generates two cell populations: TE cells expressing *Cdx2* and ICM cells expressing the *Oct4* gene (Chazaud and Yamanaka, 2016). We examined the first cell fate decision by immunostaining for Oct4 and *Cdx2* at E3.75. There was no difference in TE and ICM cell allocation between *dF/+* and *dKO/+* embryos (Fig. S5A). Neither the number of ICM and TE cells nor their ratio was significantly changed, although the number of cells expressing both factors was increased in *dKO/+* embryos (Fig. S5B,C). Thus, the first cell fate decision appears to be normal in embryos with maternal *Ezh1/2* deletion.

The second cell lineage decision, occurring during implantation, segregates the ICM into EPI cells and primitive endoderm (PrE) cells that express *Nanog* and *Gata6*, respectively (Chazaud and Yamanaka, 2016). EPI cells produce the fetus, while the PrE cells and trophoblast produce extra-embryonic tissues (DePamphilis, 2016). The phenotypic similarity between *dKO/+* embryos and *Nanog* null mice at the peri-implantation period (Mitsui et al., 2003) prompted us to examine whether the loss of maternal *Ezh1/2* results in the dysregulation of the second cell fate decision. As shown in Fig. 7, the morphology of E4.5 *dKO/+* embryos was no different

from that of *dF/+* embryos at the same stage (Fig. 7A). Although the expression of *Nanog* and *Gata6* was observed in late blastocysts (Fig. 7B), *Nanog*-positive (*Nanog*⁺) cells in *dKO/+* embryos were obviously fewer in number than that in *dF/+* embryos, indicating that the number of EPI cells was reduced (Fig. 7B). Cell counts showed that the numbers of cells in *dF/+* and *dKO/+* embryos were nearly equivalent (Fig. 7C), while the number of EPI cells in *dKO/+* embryos was remarkably reduced (6.83 ± 3.24) compared with that in *dF/+* embryos (11.58 ± 3.00) (Fig. 7C). Unexpectedly, the PrE cell number was significantly decreased, to around 66% of that of *dF/+* embryos (Fig. 7C). Moreover, the ratios of both EPI and PrE were obviously reduced (Fig. 7D). The TE cell number was not significantly changed, but its ratio to the total cell number was obviously increased, while mixed-expressed cells appeared and accounted for about 4.21% of total cells (Fig. 7C,D). Consistent with this result, Oct4 and *Gata6* were expressed in late blastocysts (Fig. S6A). The average cell numbers per embryo was not changed significantly (Fig. S6B), but the number of Oct4-only⁺ cells was obviously decreased in *dKO/+* embryos at E4.5 (Fig. S6C,D). These results show that maternal *Ezh1/2* deletion impaired the second cell fate decision, leading to fewer EPI cells and more cells with mixed stem cell marker expression during implantation.

It has been shown that the promoters of developmental genes are strongly marked with H3K27me3 in EPI in post-implantation embryos (Rugg-Gunn et al., 2010; Zheng et al., 2016). Therefore, we hypothesized that the defects in second lineage commitment may be associated with reduced H3K27me3 signals. To test this hypothesis, we examined H3K27me3 modification and *Nanog* expression in embryos at E4.5. In addition to punctate H3K27me3 signals in some embryos, H3K27me3 modification appeared in *Nanog*⁺ cells and was apparently reduced in *dKO/+* embryos and almost absent in *Gata6*⁺ cells of both *dF/+* and *dKO/+* late blastocysts (Fig. 7E and Fig. S7C). We found strong correlations between *Nanog*⁺ cells and H3K27me3 modification in both *dF/+*

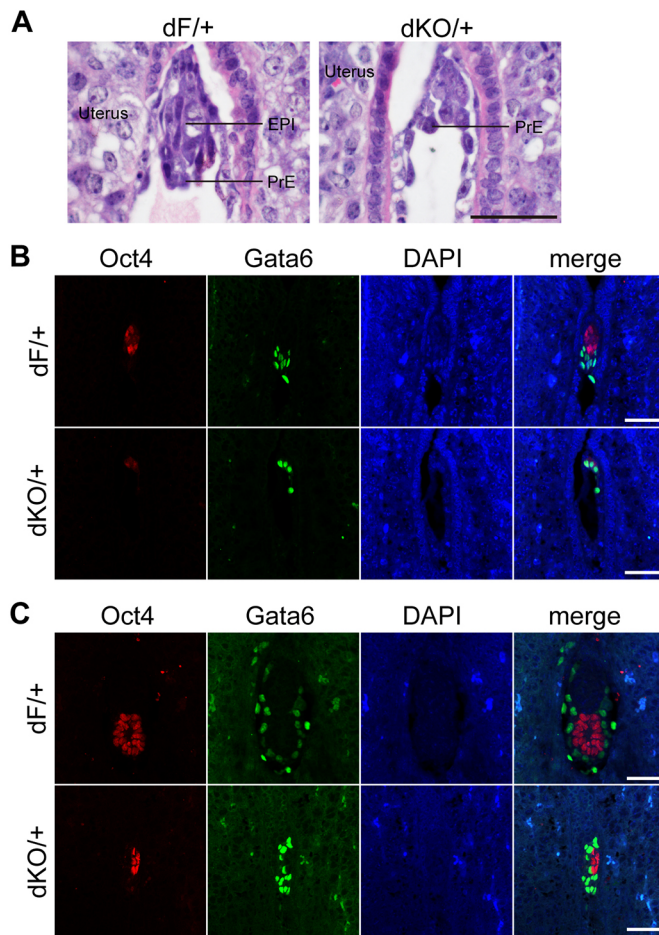


Fig. 6. Developmental defects of epiblasts in post-implantation dKO/+ embryos. (A) Hematoxylin and Eosin staining of uterine decidua sections at E4.75. Scale bar: 50 μm. EPI, epiblast; PrE, primitive endoderm. (B) The expression of Oct4 and Gata6 in embryos at E4.75 by immunofluorescent (IF) staining. Scale bars: 50 μm. (C) The expression of Oct4 and Gata6 in embryos at E5.5 by IF staining. Scale bars: 50 μm. Epiblast (EPI) cells are marked by Oct4 (red). Primitive endoderm (PrE) cells, visceral endoderm (VE) cells and parietal endoderm (PE) cells are marked by Gata6 (green).

and dKO/+ embryos (Fig. S7D). However, the number of Nanog⁺ and H3K27me3⁺ cells was not notably different between sF/+ and sKO/+ late blastocysts, although they exhibited an obvious correlation in both sF/+ and sKO/+ embryos (Fig. S8). These observations suggested that EPI development is associated with H3K27me3 modification. In summary, the maternal *Ezh1/2* is crucial for second cell lineage determination and propagation of the EPI state during implantation.

Identifying differentially expressed genes and putative imprinted genes in dKO/+ embryos

To further examine how maternal *Ezh1/2* KO caused embryonic growth arrest, we performed RNA-seq at the morula stage and E7.5 (Fig. 8A,B). Few DEGs were identified in morulae, whereas thousands of DEGs were found in both the EPI and extra-embryonic ectoderm (ExE) at E7.5 (Fig. 8C). GO analysis showed that many DEGs were enriched in the stem cell population and over the course of embryonic development (Fig. 8D). The expression of essential genes associated with stem cell identity and embryonic development, such as *Fgf4* and *Sox2* in EPI and *Cdx2*, *Ascl2* and *Slc34a2* in ExE, were remarkably decreased (Fig. 8E). This result

indicates that embryonic arrest is probably caused by stem cell defects.

Previous studies have demonstrated that maternal KO of *Eed* causes embryonic lethality and loss of H3K27me3 imprinting (Inoue et al., 2018). To investigate whether maternal *Ezh1/2* KO also causes a loss of H3K27me3 imprinting, we performed PN exchange and RNA-seq (Fig. 8A,B). Although only a few DEGs were discovered in the morula, one of these genes, *Rlim*, which is involved in random inactivation of X chromosome (Barakat et al., 2011; Shin et al., 2010), was decreased expressed (LogFC=−1.4065 and FDR=0.042762) (Fig. 8B). This prompted us to analyze the gene expression of X chromosome genes. Genes on the X chromosome were specifically downregulated (Fig. 8F). Thus, the X chromosome inactivation may be affected by maternal *Ezh1/2* KO. To examine the allelic gene expression and to screen putative H3K27me3-dependent imprinted genes, we performed RNA-seq on PN exchanged morulas (Fig. 8A,B). Eighty genes, including *Xist*, *Gras1b* and *Epas1*, were identified as putative H3K27me3-dependent imprinted genes (Fig. 8G and Table S4). To examine the allelic H3K27me3 modification of these genes, ChIP-seq data from maternal *Eed* KO (Inoue et al., 2018) were used. Among the 80 genes, 26 showed maternal H3K27me3 modification at their promoters (Table S4). These results suggest that maternal *Ezh1/2* KO caused a loss of H3K27me3-dependent imprinting.

DISCUSSION

Our study investigated the effects of maternal *Ezh1/2* on H3K27 methylation patterns and mouse embryonic development by deleting *Ezh1* and *Ezh2* in oocytes. We reveal that *Ezh2* is required for H3K27me3, and that *Ezh1* partially complements *Ezh2* for H3K27me2 in oocytes. The effect of maternal *Ezh1/2* was inherited in descendant embryos. Loss of maternal *Ezh1/2* causes a delay in the restoration of H2K27me2/3 modification in pre-implantation embryos *in vivo*. We also demonstrated that the loss of maternal *Ezh1/2* has long-term developmental consequences, resulting in growth retardation. Maternal *Ezh1/2* is essential for second lineage determination and EPI cell fate during implantation. Crucial developmental genes were dysregulated in post-implantation embryos, and putative H3K27me3-dependent imprinted genes were identified. These findings uncover the essential function of maternal *Ezh1/2* on H3K27me2/3 modification and embryonic development, providing a novel understanding of embryonic development regulation by epigenetic modulators.

Maternal *Ezh1* and *Ezh2* in descendant development in mice

It has been shown that *Ezh1* and *Ezh2* are functionally redundant (Ezhkova et al., 2009; Margueron et al., 2008; Shen et al., 2008), and tissues deficient in *Ezh1* and *Ezh2* show more severe defects than those lacking only *Ezh2* (Ezhkova et al., 2011; Mochizuki-Kashio et al., 2015). This is also the case in our work. Previous reports indicated that mice lacking *Ezh1* were normal (Ezhkova et al., 2011), while oocyte-specific deletion of *Ezh2* induced growth retardation in offspring but did not influence mouse fertility (Erhardt et al., 2003), which is consistent with the fertility performance of dCtrl and sKO females in the present work. In our mouse model, double knockout of *Ezh1* and *Ezh2*, but not *Ezh1* or *Ezh2* alone, in oocytes caused embryonic sublethality, suggesting that *Ezh1* complements (or partially complements) *Ezh2* function in embryonic development, and that maternal *Ezh2* and *Ezh1* working together governs descendant development. Notably, the patterns of H3K27me3 in late blastocysts and the breeding results were

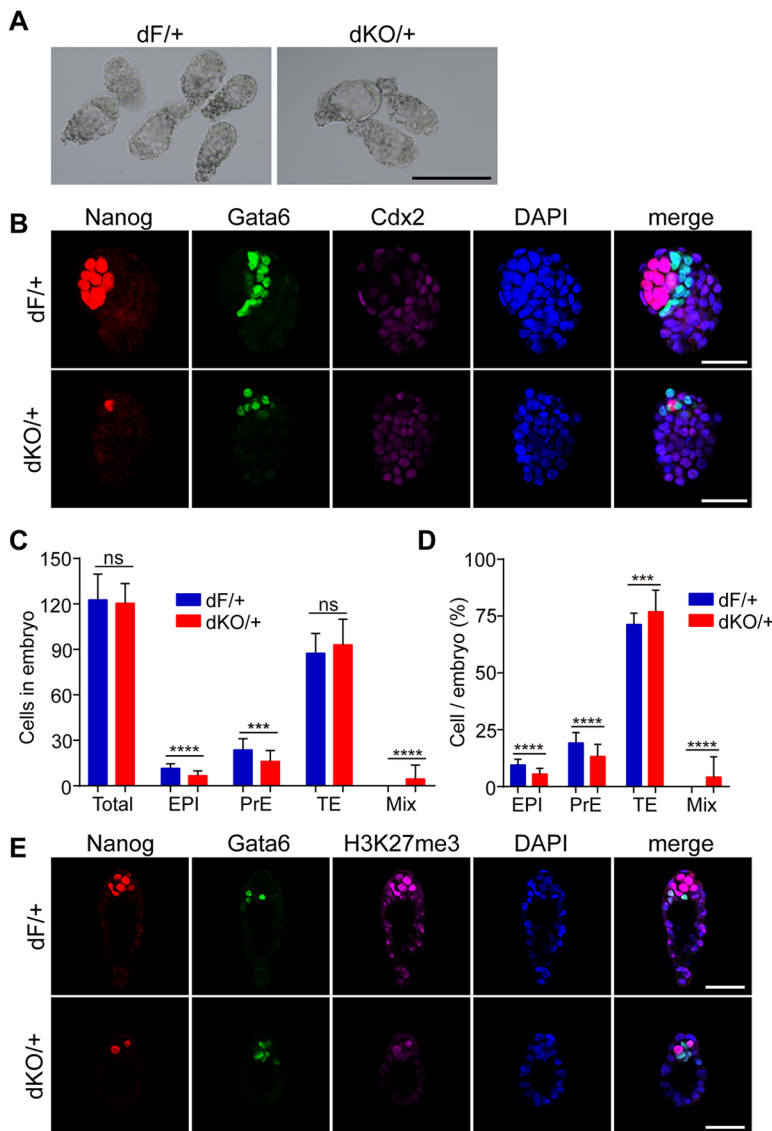


Fig. 7. Decreased numbers of epiblast cells in dKO/+ embryos at E4.5. (A) Representative images of flushed embryos at E4.5. Scale bar: 50 μ m. (B) Representative images of stem cell distribution in late blastocysts at E4.5. EPI cells were stained for Nanog (red), PrE cells were stained for Gata6 (green) and TE cells were stained for Cdx2 (magenta). Total number of embryos: dF/+, $n=31$; dKO/+, $n=35$. Scale bars: 50 μ m. (C) The number of different cell parts in embryos. Data are mean \pm s.d. Statistical comparisons of values were made using the Mann-Whitney test (Total, EPI, PrE and Mix) or an unpaired t -test (TE). ns, not significant; *** $P<0.001$; **** $P<0.0001$. (D) The ratio of different cell parts. Data are mean \pm s.d. Statistical comparisons of values between dF/+ and dKO/+ were made using Student's t -test. ns, not significant; *** $P<0.001$; **** $P<0.0001$. (E) Single optical sections of late blastocysts immunostained for Nanog, Gata6 and H3K27me3. Number of embryos: dF/+, $n=11$; dKO/+, $n=7$. Scale bars: 50 μ m.

consistent to some extent. Considering that H3K27me3 modification is associated with pluripotent EPI, it is possible that the pattern of H3K27me3 during the peri-implantation period may determine the embryonic development potential, which might explain the fertility discrepancy between different groups.

Maternal *Ezh1* and *Ezh2* in H3K27 methylation in pre-implantation embryos *in vivo*

Our knockout mouse model showed that *Ezh2* is required for H3K27me3 and that *Ezh1* complements *Ezh2* in H3K27me2 in oocytes. The effect of *Ezh1/2* is inherited in maternal knockout zygotes. H3K27me3 was lost in the sKO/+ and dKO/+ maternal PN whereas H3K27me2 was reduced in the sKO/+ female PN but absent in the dKO/+ female PN. The H3K27me2 signal was almost undetectable in both the paternal and maternal PN in the dKO/+ zygotes, similar to the H3K27me2 pattern in Eed m-p/+ zygotes, but different from a previous report in which the H3K27me2 of maternal PN was normal in *Ezh2*m-p/+ *Ezh1* siRNA zygotes (Meng et al., 2020). In addition, the asymmetric parental H3K27me2/3 signal in the PNs of sF/+ and dF/+ zygotes is consistent with previous reports (Huang et al., 2014; Santos et al.,

2005). Interestingly, similar patterns of H3K27me3 and H3K27me2 signals appeared in the paternal PN of maternal KO zygotes in this work. Normally, the histones in the paternal PN are initially hypomethylated and gradually acquire H3K27me2/3 modifications in late zygotes due to a preferential recruitment of the PRC2 complex to maternal PNs; these marks become apparent in the paternal PN at later stages (Burton and Torres-Padilla, 2010; Erhardt et al., 2003). The lost deposition of H3K27me2/3 in the paternal PN of KO/+ zygotes indicates that the PRC2 complex is inactive in late zygotes or at least absent in the paternal PN. According to the results in our study, we speculate that *Ezh1* and *Ezh2* are required for *de novo* H3K27me2 in oocytes, which could be restored and inherited in the maternal PN in zygotes.

Deficiency of *Ezh1* does not affect H3K27me2/3 patterns, whereas the loss of maternal *Ezh2* alone or in combination with *Ezh1* leads to delayed restoration of H3K27me2/3 in pre-implantation embryos *in vivo*, indicating that maternal *Ezh2* has a long-term effect on H3K27me2/3 in early embryos. However, the loss of H3K27me3 induced by *Ezh2* single maternal KO did not affect embryo development. Potential explanations for this observation are as follows:

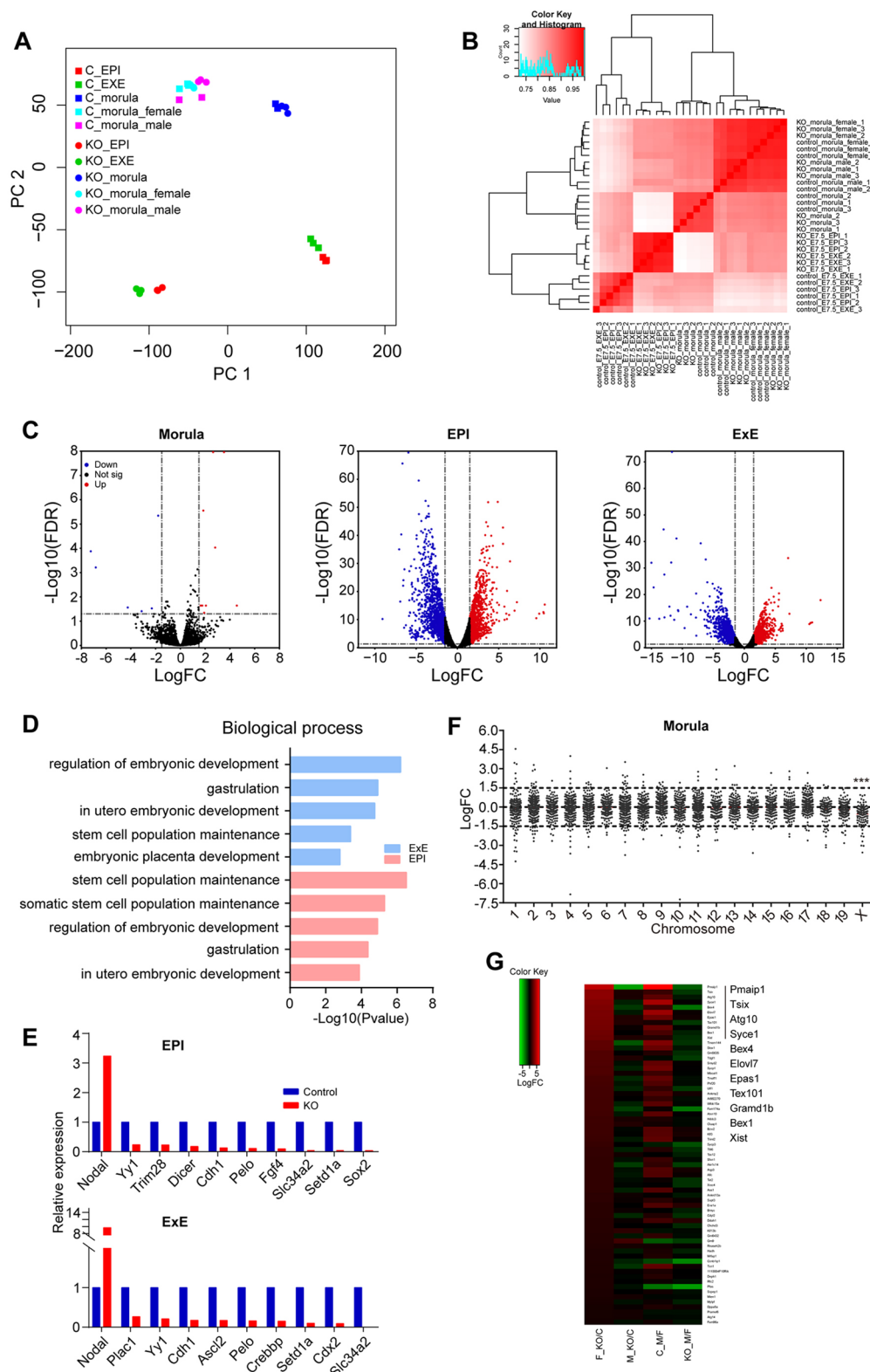


Fig. 8. Transcriptomes and putative imprinted genes in dKO/+ embryos. (A) Principal component analysis (PCA) comparison between all samples. (B) Correlation between biological replicates of RNA-seq samples. Control_morula, Control_E7.5_EPI and Control_E7.5_ExE are from dF/+ embryos. KO_morula, KO_E7.5_EPI and KO_E7.5_ExE are from dKO/+ embryos. Control_morula_male and Control_morula_female are from pronucleus exchange of dF/+ zygotes. KO_morula_male and KO_morula_female are from pronucleus exchange of dKO/+ zygotes. (C) Volcano plot comparing RNA transcripts in control and KO embryos. Cutoff: FDR<0.05 and |logFC|>1.5. Data were plotted by Bioinformatics (<http://www.bioinformatics.com.cn>). (D) Biological process associated with stem cells and development at E7.5. GO was analyzed in Metascape. (E) Relative expression levels of genes associated with stem cells and development by RNA-seq at E7.5. The expression level of the control was set as 1. (F) Relative gene expression levels of morula from chromosomes 1 to X (excluding Y). One-way ANOVA test: ****P<0.0001. (G) Heatmap showing putative H3K27me3-dependent imprinted genes at the morula stage. C, control; F, female; M, male.

(1) H3K27me3 is still enriched in the locus of imprinted genes, despite the loss of H3K27me3 staining; in this case, Ezh1 may safeguard this modification. H3K27me2/3 status in dKO/+ embryos is severely delayed compared with that in sKO/+, supporting this hypothesis and suggesting that Ezh1 compensates to sustain some residual PRC2 activity (Mochizuki-Kashio et al., 2015).

(2) Imprinting is lost from some genes that are not crucial to development.

(3) Extra epigenetic regulators probably guard the imprinting of crucial genes in Ezh2 KO. These hypotheses are all need to be investigated.

However, the H3K27me2/3 patterns in *in vivo* pre-implantation embryos in our study are different from those in previous reports (Erhardt et al., 2003; Inoue et al., 2018; Meng et al., 2020). H3K27me3 was not recovered in early blastocysts of sKO/+ and dKO/+ embryos in our research. Erhardt et al. showed that a normal H3K27me3 pattern emergence in maternal Ezh2 knockout embryos (16-cell stage), but after the time of embryonic Ezh2 activation (Erhardt et al., 2003), whereas H3K27me3 of maternal Eed knockout embryos becomes comparable at the morula stage (Inoue et al., 2018). This difference may be attributable to differences in the collections of embryos, as histone modification may be changed by *in vitro* operation and culture (Kohda, 2013); alternatively, activation of Ezh1/2 may occur later than activation of Eed in maternal knockout embryos. Additionally, the conversion to histone methylation to H3K27me3 is more time-consuming than conversion of H2K27me1 and H3K27me2 (Laugesen et al., 2019), and recent work indicates that H3K27me2 might be a crucial prerequisite for *de novo* H3K27me3 (Meng et al., 2020). Therefore, the delayed restoration of H3K27me3 may be induced by deferred H3K27me2. In dKO/+ pre-implantation embryos, H3K27me2 appeared from the morula stage onwards and completely recovered at the late blastocyst stage. As Ehmt1 is also involved in the establishment of H3K27me2 (Meng et al., 2020), we suggest that this may be associated with delayed embryonic Ezh1/2 or Ehmt1 transcription to initiate H3K27me2. This hypothesis should be verified in the future work. Above all, it can be stated that the capacity of H3K27 methylation reprogramming in pre-implantation embryos was compromised by the deletion of maternal Ezh2 alone or in combination with Ezh1.

Maternal PRC2-H3K27me3 in the second cell fate decision and embryonic development

Erhardt et al. suggested that Ezh2 may be crucial for the propagation of pluripotency and for cell fate determination during the early stages of embryonic development (Erhardt et al., 2003). In this work, we reveal that maternal loss of Ezh1/2 leads to a reduction in EPI cell number and defective second cell fate specification during implantation, revealing the importance of Ezh1/2 and H3K27me3 for the EPI state and cell fate decisions. Therefore, the fact that stem cells from Ezh2 mutant embryos are difficult to establish and show impaired potential for outgrowth (O'Carroll et al., 2001) may be associated with pluripotency failure of EPI cells due to a lack of Ezh2 and H3K27me3.

It is now clear that a reduction in ICM cell numbers diminishes embryogenetic potential (Tam, 1988). The initiation of gastrulation is suggested to require the attainment of some threshold, either a minimum cell number or a certain tissue mass of EPI (Kojima et al., 2014). Our results showed a markedly decrease in the number of ICM/EPI cells in dKO/+ embryos during implantation. Fgf4 and Sox2 are pluripotency markers associated with both pre- and post-implantation EPI (Boroviak et al., 2015). Moreover, Oct4 and

Sox2 collaboratively induce the expression of genes essential for maintaining pluripotency, Nanog and Fgf4 (Rizzino and Wuebben, 2016), and their own expression. Considering the reduced number of Oct4-only⁺ and Nanog-only⁺ cells during the peri-implantation phase and decreased expression of Fgf4 and Sox2 post-implantation, it is suggested that the Sox2, Oct4, Nanog and Fgf4 feedback loop is disrupted, resulting in embryo loss and growth retardation during gastrulation. It is worth mentioning that the *in vitro* culture (IVC) system is a powerful tool for visualizing the development of the EPI and its surrounding tissues through the implantation stages (Bedzhov and Zernicka-Goetz, 2014; Morris et al., 2012). By using this system, the dynamics of blastocyst transformation into the egg cylinder will be directly revealed.

In our study, EPI cells (Nanog⁺) possessed H3K27me3 signals at E4.5 in both dF/+ and dKO/+ embryos. Similar H3K27me3 patterns were observed in previous reports (Erhardt et al., 2003; Liu et al., 2019). In ESCs, a set of genes are bivalently modified with H3K4me3 and H3K27me3, and remain 'poised' (Liu et al., 2016; Rugg-Gunn et al., 2010). The withdrawal of PRC2 core components and H3K27me3 methylation results in bivalent derepression of genes and abnormal differentiation (Azuara et al., 2006; Boyer et al., 2006; Jørgensen et al., 2006; Lee et al., 2006). Considering the H3K27me3 modifications of developmental genes in EPI cells (Rugg-Gunn et al., 2010; Zheng et al., 2016), the decrease in Nanog⁺ cells may result from the deficiency of H3K27me3 and the derepression of cell fate-specific factors, which lead to differentiation into other lineages. A recent report demonstrated that in mouse ESCs, Nanog blocks differentiation by maintaining the H3K27me3 modification at developmental regulators (Heurtier et al., 2019). However, whether this regulatory network functions *in vivo* remains to be addressed in detail. For the two rounds of cell fate specification, cells in the wrong position or with ectopic expression of the transcriptional profile will eventually be cleared out by apoptosis (Zhu and Zernicka-Goetz, 2020). Whether the decreased number of ICM (EPI and PrE) cells is associated with increased apoptosis needs further assessment. In brief, the loss of maternal Ezh1/2 and delayed restoration of H3K27 methylation change the epigenetic plasticity of pluripotent cells.

Maternal Ezh1/2 and gene imprinting in placental development

In maternal Ezh1/2 double KO mice, the development defects of the fetuses and placentas fell into three distinct categories. The cause of phenotypic variation may be related to epigenetic modification of maternal PRC2 on fetal and placental development (Kohda, 2013; Lee et al., 2006). The process involves multiple factors, including the imprinting of many genes and the development of multiple cell types (Jambhekar et al., 2019; Jørgensen et al., 2006; Mei et al., 2021). Therefore, the long-term effects of maternal Ezh1/2 KO may vary based on the context in each embryo. The placental failure in our study is likely caused by multiple factors. It is known that a lack of chorioallantoic attachment and branching results in placental failure and embryonic mortality (Rossant and Cross, 2001; Walentin et al., 2016). Hence, in our work, failure of placentation in mid-gastrulation is at least one of the reasons for embryonic loss. But, it is not clear how the loss of maternal Ezh1/2 leads to chorioallantoic attachment failure; this error might be a by-product of additional mechanisms (Inoue et al., 2018; Perez-Garcia et al., 2018). Fgf4 is expressed by EPI during implantation development and is necessary for trophoblast stem cell proliferation (Boroviak et al., 2015; Christodoulou et al., 2019; Tanaka et al., 1998). Thus, the

diminished Cdx2 in ExE at E7.5 and placental failure may be caused by lower Fgf4 in EPI, which is a secondary effect of maternal *Ezh1/2* KO. Additionally, *Mash2* (*Ascl1*) mutants die from placental failure at around E10, and in *Slc38a2* mutants, the placental labyrinth is absent (Guillemot et al., 1994; Shibasaki et al., 2009).

H3K27me3-modified imprinted genes are found to play important roles in placental development (Inoue et al., 2020). Several imprinted genes, including *Slc38a4*, *Sfmbt2* and *Gab1*, remain in their imprinted state in the placenta (Inoue et al., 2018). Deletion of these gene in mouse causes the defect of placenta and fetus (Mei et al., 2021). Here, we have also obtained 80 putative H3K27me3-dependent imprinted genes in our *Ezh1/2* maternal KO morulas. So far, there are no other report on the H3K27me3 imprinting genes in *Ezh1/2* or *Ezh2* maternal KO embryos. But the H3K27me3-dependent imprinted genes have been analyzed in maternal *Eed* KO mouse embryos, and 26 of H3K27me3-dependent imprinted genes in our study were maternally marked according to their ChIP-seq data (Inoue et al., 2018). Three of these genes (*Xist*, *Grm1b* and *Epas1*) were also reported to be imprinted by Inoue et al. (2018), indicating that maternal *Ezh1/2* KO could lead to loss of H3K27me3-dependent imprinting.

In contrast, placental enlargement was observed during the later development of dKO/+ embryos, characterized by expansion of the spongiotrophoblast layer. This phenotype was also reported in mouse embryos generated by somatic cell nuclear transfer (SCNT) (Tanaka et al., 2001). Some recent reports have demonstrated that the loss of H3K27me3 imprinting during SCNT contributes to placentomegaly in SCNT embryos, and that a more normal placenta weight could be restored by regulating H3K27me3-imprinted genes (Inoue et al., 2020; Matoba et al., 2018; Wang et al., 2020; Xie et al., 2022). However, placental enlargement is suggested to be associated with the PRC1 complex, which guides the maternal inheritance and deposition of H3K27me3 in embryos (Chen et al., 2021; Mei et al., 2021).

MATERIALS AND METHODS

Animals

Unless otherwise stated, the mice used in this study were of mixed background (129/SvJ and C57BL/6). The *Ezh2 loxp* and *Ezh1^{-/-}* mice were gifts from Professor Alexander Tarakhovskiy (The Rockefeller University, New York, USA). The mice were housed at Xiamen University Laboratory Animal Center under a 12 h light-dark cycle. Food and water were available *ad libitum* and room temperature was 24°C with controlled humidity. All animal work was undertaken in accordance with the Xiamen University Animal Ethics Committee (approval number 2015014). Genotyping was performed from tail DNA. Primers for genotype are shown in Table S2.

Fertility studies

Fertility studies were performed as previously described (Andreu-Vieyra et al., 2008). To evaluate reproductive performance, individually caged females (2 months old) were bred with adult wild-type males (C57BL/6J) of known fertility. After delivery, the number of pups was recorded. On the seventh day, the pups were removed, and the females and males continued to cage together. The breeding experiment lasted 6 months. The number of litters and the number of pups were recorded during fertility study period.

Mating, implantation, embryo collection and decidua dissection

For basic embryological analyses, adult dCtrl and dKO females were naturally mated with adult wild-type males (C57BL/6J). The morning on which a plug was found was counted as embryonic day 0.5 (E0.5) or day 1 of pregnancy. Implantation sites on day 5 (09:00 am) of pregnancy were visualized by an intravenous injection of Chicago Blue dye solution.

Blastocysts were flushed from the uterine horn with M2 medium at E3.75 and E4.5. Deciduae of pregnant females were dissected from E4.75–E10.5. The fetuses and placentas were collected and dissected carefully under a stereoscope at E10.5 and E17.5.

Histology, immunohistochemistry and immunofluorescence

Tissues were fixed in 4% paraformaldehyde (PFA), dehydrated in ethanol, embedded in paraffin wax, and sectioned (5 µm). For tissue morphology observation, sections were stained with Hematoxylin and Eosin (HE). For immunohistochemistry, sections were treated with 3% H₂O₂ for 20 min after antigen retrieval, followed by blocking for 1 h in 5% bovine serum albumin (BSA). Sections incubated in primary antibodies overnight at 4°C were subsequently treated with PV-9001 kits (ZSBI) before being exposed to diaminobenzidine (DAB). Finally, sections were counterstained with Hematoxylin. For immunofluorescence, after antigen retrieval, sections were blocked in 5% bovine serum albumin or 5% donkey serum and then incubated in primary antibodies overnight at 4°C. The sections were then washed in wash buffer and incubated with the appropriate Alexa-Fluor-conjugated secondary antibodies at 37°C for 1 h. After staining with DAPI (Vector Laboratories), the samples were analyzed using confocal microscopy (Zeiss LSM 780). The antibodies are listed in Table S3.

Oocyte and early embryo collection

MII oocytes were collected from females (3–5 weeks old) that have been superovulated by injection with PMSG and hCG (San-Sheng Pharmaceutical). Pre-implantation embryos were collected from superovulated females mated with adult wild-type males (C57BL/6). Each set of embryos at a particular stage was flushed from the reproductive tract at defined time periods after hCG administration: 20 h (MII oocyte), 27–28 h (late zygote), 48 h (late 2-cell), 54–56 h (4-cell), 68–70 h (8-cell), 80 h (morula), 90–96 h (early blastocyst) and 120 h (late blastocyst).

Whole-mount immunostaining

Oocytes and embryos were fixed in 4% PFA containing 0.1% BSA for 20 min at room temperature. After that, all fixed samples were washed with PBS containing 0.1% BSA and permeabilized in 0.1% Triton X-100 in PBS with 0.1% BSA at room temperature for 30 min, and blocked in 1% BSA or 5% donkey serum in PBS at room temperature for 1 h. Blocked oocytes and embryos were incubated with primary antibodies at 4°C overnight. Secondary antibodies were incubated at 37°C for 1 h. After washing, the oocytes and embryos were mounted on a glass slide in DAPI. Fluorescence was detected under a laser-scanning confocal microscope (Zeiss, LSM 780).

Antibody labeling

A 4AF647R-Antibody conjugation Kit (4A Biotech) was used to label H3K27me3 antibody with 4AF647R dyes. According to the labeling protocol, H3K27me3 antibody solutions (CST, 9733) were concentrated by ultrafiltration and resuspended in PBS to 0.5–1 mg/ml, as indicated by the labeling protocol. An appropriate amount of antibody to be labeled was transferred to a clean tube. A 1/10 volume of reaction buffer was added to the tube with antibody and then mixed well. The vial was incubated in the dark for 30 min at room temperature. Labeled antibody solution was diluted with storage buffer, and stored in single use aliquots at –20°C. When performing immunofluorescence, labeled H3K27me3 was used after standard immunofluorescence staining with primary and secondary antibodies.

Quantitative real time PCR (QPCR) analyses

Oocyte preparation was performed as reported previously (Kim et al., 2015). RNA from oocytes was isolated using the SuperPrep Cell Lysis & RT Kit for real-time PCR (TOYOBO, Osaka, Japan). PCR was performed on the Agilent AriaMx Real-Time PCR System. Primers are listed in Table S2. The relative transcripts amount was calculated by the cycle threshold method described by Agilent using the AtiaMx Real-Time PCR System Software and normalized to the endogenous reference (β -actin). The relative amount of target gene expression for each sample was calculated and plotted as the mean \pm s.d.

Western blot analyses

Western blotting was carried out as previously described (Kim et al., 2015). Equal numbers of oocytes were collected in PBS containing 0.1% BSA. Proteins were isolated by centrifuging the oocytes at 12,000 *g* for 15 min at 4°C. The protein samples were then mixed and treated with 2×SDS buffer containing protease inhibitor. The protein molecules were separated by gel electrophoresis and transferred onto PVDF membranes. The membranes were blocked in 5% milk in TBST and then incubated with primary antibodies, followed by washing then incubation with secondary antibodies. The band was detected with a Bio-Rad imaging system.

Vasectomy

Vasectomy was operated as previous documented (Bermejo-Alvarez et al., 2014). Wild-type male mice (CD1) with a proven mating performance were selected and anesthetized. The abdomen surface was cleaned and wiped with 70% ethanol and then opened, and the vas deferens was exposed by gripping the testicular adipose pad with forceps. The vas deferens was cut and cauterized at two points simultaneously by using flamed dressing forceps. The testicle, epididymis and vas deferens were moved back to the abdominal cavity, and the procedure was repeated for the other side. The muscle and skin were sutured. The vasectomized male was moved to the cage placed on a warm stage and observed until it recovered from anesthesia. Wound clips were removed 14 days after vasectomy. The infertility of the vasectomized male was tested by mating fertile females before using them to obtain recipients (pseudopregnant female mice that were produced to mate with vasectomized male mice and received the blastocysts from the embryo transfer experiment).

Embryo transfer

Embryo transfer was performed as previously described (Bermejo-Alvarez et al., 2014). Female mice were superovulated and mated with wild-type males (C57BL/6). Blastocysts were flushed out of the uteri on day 4 of pregnancy, then transferred into the uteri of pseudopregnant female mice (CD1, wild type) mated with vasectomized males. About 17 days after embryo transfer, the recipients were examined for the presence of a fetus. The number of fetuses was recorded.

RNA-seq library preparation and sequencing

Libraries for RNA-seq were constructed with Smart-seq2 (Picelli et al., 2014). Cells were washed at least three times with 0.5% BSA-PBS and selected into lysis buffer by mouth pipetting. After cell lysis and reverse transcription, the cDNA was amplified for 18 cycles in a thermal cycler. The products were fragmented with a Covaris S220 instrument, and the libraries were constructed with a Kapa Hyper Prep kit (KAPA KK8504). The libraries were sequenced on an Illumina HiSeq 2500 with 125 bp single end sequencing, and quality control was performed by Berry Genomics. RNA-seq data processing was performed according to a previous report (Liu et al., 2016). ChIP-seq data (GSE116713) were downloaded from GEO (Inoue et al., 2018).

Analysis of H3K27me3 imprinting genes

We performed RNA-seq on PN-exchanged morulas and identified the putative H3K27m3-dependent imprinted genes according to the expression of genes in different PN exchanged morulas. A H3K27m3-dependent imprinted genes should have the following: (1) low expression in wild-type female PN-exchanged morulas, but high expression in wild-type male PN-exchanged morulas; (2) clearly lower expression in wild-type female PN-exchanged morulas than in female *Ezh1/2* KO (dKO) PN-exchanged morulas; and (3) no difference in the expression in male PN-exchanged morulas between wild type and dKO.

Statistical analyses and data visualization

Statistical analyses were performed in GraphPad Prism 7. The quantitative data presented show the mean±s.d., percentages or the total number of data points obtained. Levels of significance were calculated using the Mann–Whitney test, an unpaired *t*-test or a χ^2 test. In all figures: ns, not significant; **P*<0.05; ***P*<0.01; ****P*<0.001; *****P*<0.0001.

Acknowledgements

We gratefully thank Professor Alexander Tarakhovsky at Rockefeller University (New York, USA) for the gift of transgenic mice.

Competing interests

The authors declare no competing or financial interests.

Author contributions

Conceptualization: Z.L.; Methodology: Y.Z., D.B., D.Z., Y.T.; Validation: J.L.; Formal analysis: Y.Z., Y.W., J.L.; Investigation: Y.Z., D.B., Y.W., D.Z., M.L.; Data curation: D.B., Y.W., J.L., S.G.; Writing - original draft: Y.Z., Z.L.; Writing - review & editing: S.G., Z.L.; Visualization: S.G.; Supervision: H.W., Z.L.; Project administration: H.W., Z.L.; Funding acquisition: H.W., Z.L.

Funding

This work was supported by the National Key Research and Development Program of China (2018YFC1003701 and 2017YFC1001402) and the National Natural Science Foundation of China (31970797 and 31671564).

Data availability

RNA-seq data have been deposited in SRA under accession number PRJNA858919.

Peer review history

The peer review history is available online at <https://journals.biologists.com/dev/article-lookup/doi/10.1242/dev.200316>.

References

- Andreu-Vieyra, C., Chen, R. and Matzuk, M. M. (2008). Conditional deletion of the retinoblastoma (Rb) gene in ovarian granulosa cells leads to premature ovarian failure. *Mol. Endocrinol.* **22**, 2141–2161. doi:10.1210/me.2008-0033
- Azuara, V., Perry, P., Sauer, S., Spivakov, M., Jørgensen, H. F., John, R. M., Gouti, M., Casanova, M., Warnes, G., Merkenschlager, M. et al. (2006). Chromatin signatures of pluripotent cell lines. *Nat. Cell Biol.* **8**, 532–538. doi:10.1038/ncb1403
- Barakat, T. S., Gunhanlar, N., Pardo, C. G., Achame, E. M., Ghazvini, M., Boers, R., Kenter, A., Rentmeester, E., Grootegoed, J. A. and Gribnau, J. (2011). RNF12 activates Xist and is essential for X chromosome inactivation. *PLoS Genet.* **7**, e1002001. doi:10.1371/journal.pgen.1002001
- Bedzhov, I. and Zernicka-Goetz, M. (2014). Self-organizing properties of mouse pluripotent cells initiate morphogenesis upon implantation. *Cell* **156**, 1032–1044. doi:10.1016/j.cell.2014.01.023
- Bermejo-Alvarez, P., Park, K.-E. and Telugu, B. P. (2014). Utero-tubal embryo transfer and vasectomy in the mouse model. *J. Vis. Exp.* **84**, e51214. doi:10.3791/51214
- Boroviak, T., Loos, R., Lombard, P., Okahara, J., Behr, R., Sasaki, E., Nichols, J., Smith, A. and Bertone, P. (2015). Lineage-Specific Profiling Delineates the Emergence and Progression of Naïve Pluripotency in Mammalian Embryogenesis. *Dev. Cell* **35**, 366–382. doi:10.1016/j.devcel.2015.10.011
- Boyer, L. A., Plath, K., Zeitlinger, J., Brambrink, T., Medeiros, L. A., Lee, T. I., Levine, S. S., Wernig, M., Tajonar, A., Ray, M. K. et al. (2006). Polycomb complexes repress developmental regulators in murine embryonic stem cells. *Nature* **441**, 349–353. doi:10.1038/nature04733
- Bracken, A. P., Dietrich, N., Pasini, D., Hansen, K. H. and Helin, K. (2006). Genome-wide mapping of Polycomb target genes unravels their roles in cell fate transitions. *Genes Dev.* **20**, 1123–1136. doi:10.1101/gad.381706
- Burton, A. and Torres-Padilla, M.-E. (2010). Epigenetic reprogramming and development: a unique heterochromatin organization in the preimplantation mouse embryo. *Brief Funct. Genomics* **9**, 444–454. doi:10.1093/bfgp/elq027
- Canovas, S. and Ross, P. J. (2016). Epigenetics in preimplantation mammalian development. *Theriogenology* **86**, 69–79. doi:10.1016/j.theriogenology.2016.04.020
- Cao, R., Wang, L., Wang, H., Xia, L., Erdjument-Bromage, H., Tempst, P., Jones, R. S. and Zhang, Y. (2002). Role of histone H3 lysine 27 methylation in Polycomb-group silencing. *Science* **298**, 1039–1043. doi:10.1126/science.1076997
- Chazaud, C. and Yamanaka, Y. (2016). Lineage specification in the mouse preimplantation embryo. *Development* **143**, 1063–1074. doi:10.1242/dev.128314
- Chen, Z., Djekidel, M. N. and Zhang, Y. (2021). Distinct dynamics and functions of H2AK119ub1 and H3K27me3 in mouse preimplantation embryos. *Nat. Genet.* **53**, 551–563. doi:10.1038/s41588-021-00821-2
- Christodoulou, N., Weberling, A., Strathdee, D., Anderson, K. I., Timpson, P. and Zernicka-Goetz, M. (2019). Morphogenesis of extra-embryonic tissues directs the remodelling of the mouse embryo at implantation. *Nat. Commun.* **10**, 3557. doi:10.1038/s41467-019-11482-5
- DePamphilis, M. L. (2016). Preface. *Curr. Top. Dev. Biol.* **120**, xiii–xxi. doi:10.1016/S0070-2153(16)30163-6

- Erhardt, S., Su, I.-H., Schneider, R., Barton, S., Bannister, A. J., Perez-Burgos, L., Jenuwein, T., Kouzarides, T., Tarakhovsky, A. and Surani, M. A. (2003). Consequences of the depletion of zygotic and embryonic enhancer of zeste 2 during preimplantation mouse development. *Development* **130**, 4235-4248. doi:10.1242/dev.00625
- Ezhkova, E., Pasolli, H. A., Parker, J. S., Stokes, N., Su, I.-H., Hannon, G., Tarakhovsky, A. and Fuchs, E. (2009). Ezh2 orchestrates gene expression for the stepwise differentiation of tissue-specific stem cells. *Cell* **136**, 1122-1135. doi:10.1016/j.cell.2008.12.043
- Ezhkova, E., Lien, W.-H., Stokes, N., Pasolli, H. A., Silva, J. M. and Fuchs, E. (2011). EZH1 and EZH2 govern histone H3K27 trimethylation and are essential for hair follicle homeostasis and wound repair. *Genes Dev.* **25**, 485-498. doi:10.1101/gad.2019811
- Ferrari, K. J., Scelfo, A., Jammula, S. G., Cuomo, A., Barozzi, I., Stützer, A., Fischle, W., Bonaldi, T. and Pasini, D. (2014). Polycomb-dependent H3K27me1 and H3K27me2 regulate active transcription and enhancer fidelity. *Mol. Cell* **53**, 49-62. doi:10.1016/j.molcel.2013.10.030
- Guillemot, F., Nagy, A., Auerbach, A., Rossant, J. and Joyner, A. L. (1994). Essential role of Mash-2 in extraembryonic development. *Nature* **371**, 333-336. doi:10.1006/dbio.1997.8685
- Heurtier, V., Owens, N., Gonzalez, I., Mueller, F., Proux, C., Mornico, D., Clerc, P., Dubois, A. and Navarro, P. (2019). The molecular logic of Nanog-induced self-renewal in mouse embryonic stem cells. *Nat. Commun.* **10**, 1109. doi:10.1038/s41467-019-09041-z
- Huang, X.-J., Wang, X., Ma, X., Sun, S.-C., Zhou, X., Zhu, C. and Liu, H. (2014). EZH2 is essential for development of mouse preimplantation embryos. *Reprod. Fertil. Dev.* **26**, 1166-1175. doi:10.1071/RD13169
- Inoue, A., Chen, Z., Yin, Q. and Zhang, Y. (2018). Maternal Eed knockout causes loss of H3K27me3 imprinting and random X inactivation in the extraembryonic cells. *Genes Dev.* **32**, 1525-1536. doi:10.1101/gad.318675.118
- Inoue, K., Ogonuki, N., Kamimura, S., Inoue, H., Matoba, S., Hirose, M., Honda, A., Miura, K., Hada, M., Hasegawa, A. et al. (2020). Loss of H3K27me3 imprinting in the Sfmbt2 miRNA cluster causes enlargement of cloned mouse placentas. *Nat. Commun.* **11**, 2150. doi:10.1038/s41467-020-16044-8
- Jambhekar, A., Dhall, A. and Shi, Y. (2019). Roles and regulation of histone methylation in animal development. *Nat. Rev. Mol. Cell Biol.* **20**, 625-641. doi:10.1038/s41580-019-0151-1
- Jørgensen, H. F., Giadrossi, S., Casanova, M., Endoh, M., Koseki, H., Brockdorff, N. and Fisher, A. G. (2006). Stem cells primed for action: polycomb repressive complexes restrain the expression of lineage-specific regulators in embryonic stem cells. *Cell Cycle* **5**, 1411-1414. doi:10.4161/cc.5.13.2927
- Kim, J., Singh, A. K., Takata, Y., Lin, K., Shen, J., Lu, Y., Kerényi, M. A., Orkin, S. H. and Chen, T. (2015). LSD1 is essential for oocyte meiotic progression by regulating CDC25B expression in mice. *Nat. Commun.* **6**, 10116. doi:10.1038/ncomms10116
- Kohda, T. (2013). Effects of embryonic manipulation and epigenetics. *J. Hum. Genet.* **58**, 416-420. doi:10.1038/jhg.2013.61
- Kojima, Y., Tam, O. H. and Tam, P. P. L. (2014). Timing of developmental events in the early mouse embryo. *Semin. Cell Dev. Biol.* **34**, 65-75. doi:10.1016/j.semdcb.2014.06.010
- Laugesen, A., Højfeldt, J. W. and Helin, K. (2019). Molecular Mechanisms Directing PRC2 Recruitment and H3K27 Methylation. *Mol. Cell* **74**, 8-18. doi:10.1016/j.molcel.2019.03.011
- Lee, T. I., Jenner, R. G., Boyer, L. A., Guenther, M. G., Levine, S. S., Kumar, R. M., Chevalier, B., Johnstone, S. E., Cole, M. F., Isono, K. et al. (2006). Control of developmental regulators by Polycomb in human embryonic stem cells. *Cell* **125**, 301-313. doi:10.1016/j.cell.2006.02.043
- Liu, X., Wang, C., Liu, W., Li, J., Li, C., Kou, X., Chen, J., Zhao, Y., Gao, H., Wang, H. et al. (2016). Distinct features of H3K4me3 and H3K27me3 chromatin domains in pre-implantation embryos. *Nature* **537**, 558-562. doi:10.1038/nature19362
- Liu, J., An, L., Wang, J., Liu, Z., Dai, Y., Liu, Y., Yang, L. and Du, F. (2019). Dynamic patterns of H3K4me3, H3K27me3, and Nanog during rabbit embryo development. *Am. J. Transl. Res.* **11**, 430-441.
- Margueron, R. and Reinberg, D. (2011). The Polycomb complex PRC2 and its mark in life. *Nature* **469**, 343-349. doi:10.1038/nature09784
- Margueron, R., Li, G., Sarma, K., Blais, A., Zavadil, J., Woodcock, C. L., Dynlacht, B. D. and Reinberg, D. (2008). Ezh1 and Ezh2 maintain repressive chromatin through different mechanisms. *Mol. Cell* **32**, 503-518. doi:10.1016/j.molcel.2008.11.004
- Matoba, S., Wang, H., Jiang, L., Lu, F., Iwabuchi, K. A., Wu, X., Inoue, K., Yang, L., Press, W., Lee, J. T. et al. (2018). Loss of H3K27me3 imprinting in somatic cell nuclear transfer embryos disrupts post-implantation development. *Cell Stem Cell* **23**, 343-354.e5. doi:10.1016/j.stem.2018.06.008
- Matsui, Y. and Mochizuki, K. (2014). A current view of the epigenome in mouse primordial germ cells. *Mol. Reprod. Dev.* **81**, 160-170. doi:10.1002/mrd.22214
- Mei, H., Kozuka, C., Hayashi, R., Kumon, M., Koseki, H. and Inoue, A. (2021). H2AK119ub1 guides maternal inheritance and zygotic deposition of H3K27me3 in mouse embryos. *Nat. Genet.* **53**, 539-550. doi:10.1038/s41588-021-00820-3
- Meng, T.-G., Zhou, Q., Ma, X.-S., Liu, X.-Y., Meng, Q.-R., Huang, X.-J., Liu, H.-L., Lei, W.-L., Zhao, Z.-H., Ouyang, Y.-C. et al. (2020). PRC2 and EHMT1 regulate H3K27me2 and H3K27me3 establishment across the zygote genome. *Nat. Commun.* **11**, 6354. doi:10.1038/s41467-020-20242-9
- Michalak, E. M., Burr, M. L., Bannister, A. J. and Dawson, M. A. (2019). The roles of DNA, RNA and histone methylation in ageing and cancer. *Nat. Rev. Mol. Cell Biol.* **20**, 573-589. doi:10.1038/s41580-019-0143-1
- Mitsui, K., Tokuzawa, Y., Itoh, H., Segawa, K., Murakami, M., Takahashi, K., Maruyama, M., Maeda, M. and Yamanaka, S. (2003). The homeoprotein Nanog is required for maintenance of pluripotency in mouse epiblast and ES cells. *Cell* **113**, 631-642. doi:10.1016/S0092-8674(03)00393-3
- Mochizuki-Kashio, M., Aoyama, K., Sashida, K., Oshima, M., Tomioka, T., Muto, T., Wang, C. and Iwama, A. (2015). Ezh2 loss in hematopoietic stem cells predisposes mice to develop heterogeneous malignancies in an Ezh1-dependent manner. *Blood* **126**, 1172-1183. doi:10.1182/blood-2015-03-634428
- Mole, M. A., Weberling, A. and Zernicka-Goetz, M. (2020). Comparative analysis of human and mouse development: From zygote to pre-gastrulation. *Curr. Top. Dev. Biol.* **136**, 113-138. doi:10.1016/bs.ctdb.2019.10.002
- Morris, S. A., Grewal, S., Barrios, F., Patankar, S. N., Strauss, B., Buttery, L., Alexander, M., Shakesheff, K. M. and Zernicka-Goetz, M. (2012). Dynamics of anterior-posterior axis formation in the developing mouse embryo. *Nat. Commun.* **3**, 673. doi:10.1038/ncomms1671
- O'Carroll, D., Erhardt, S., Pagani, M., Barton, S. C., Surani, M. A. and Jenuwein, T. (2001). The polycomb-group gene Ezh2 is required for early mouse development. *Mol. Cell Biol.* **21**, 4330-4336. doi:10.1128/MCB.21.13.4330-4336.2001
- Perez-Garcia, V., Fineberg, E., Wilson, R., Murray, A., Mazzeo, C. I., Tudor, C., Sienerth, A., White, J. K., Tuck, E., Ryder, E. J. et al. (2018). Placentation defects are highly prevalent in embryonic lethal mouse mutants. *Nature* **555**, 463-468. doi:10.1038/nature26002
- Picelli, S., Faridani, O. R., Björklund, A. K., Winberg, G., Sagasser, S. and Sandberg, R. (2014). Full-length RNA-seq from single cells using Smart-seq2. *Nat. Protoc.* **9**, 171-181. doi:10.1038/nprot.2014.006
- Prokopuk, L., Stringer, J. M., White, C. R., Vossen, R. H. A. M., White, S. J., Cohen, A. S. A., Gibson, W. T. and Western, P. S. (2018). Loss of maternal EED results in postnatal overgrowth. *Clin. Epigenet.* **10**, 95. doi:10.1186/s13148-018-0526-8
- Rizzino, A. and Wuebben, E. L. (2016). Sox2/Oct4: A delicately balanced partnership in pluripotent stem cells and embryogenesis. *Biochim. Biophys. Acta* **1859**, 780-791. doi:10.1016/j.bbaggm.2016.03.006
- Rossant, J. and Cross, J. C. (2001). Placental development: lessons from mouse mutants. *Nat. Rev. Genet.* **2**, 538-548. doi:10.1038/35080570
- Rugg-Gunn, P. J., Cox, B. J., Ralston, A. and Rossant, J. (2010). Distinct histone modifications in stem cell lines and tissue lineages from the early mouse embryo. *Proc. Natl. Acad. Sci. USA* **107**, 10783-10790. doi:10.1073/pnas.0914507107
- Saitou, M., Kagiwada, S. and Kurimoto, K. (2012). Epigenetic reprogramming in mouse pre-implantation development and primordial germ cells. *Development* **139**, 15-31. doi:10.1242/dev.050849
- Santos, F., Peters, A. H., Otte, A. P., Reik, W. and Dean, W. (2005). Dynamic chromatin modifications characterise the first cell cycle in mouse embryos. *Dev. Biol.* **280**, 225-236. doi:10.1016/j.ydbio.2005.01.025
- Schuettengruber, B. and Cavalli, G. (2009). Recruitment of polycomb group complexes and their role in the dynamic regulation of cell fate choice. *Development* **136**, 3531-3542. doi:10.1242/dev.033902
- Shen, X., Liu, Y., Hsu, Y.-J., Fujiwara, Y., Kim, J., Mao, X., Yuan, G.-C. and Orkin, S. H. (2008). EZH1 mediates methylation on histone H3 lysine 27 and complements EZH2 in maintaining stem cell identity and executing pluripotency. *Mol. Cell* **32**, 491-502. doi:10.1016/j.molcel.2008.10.016
- Shibasaki, Y., Etoh, N., Hayasaka, M., Takahashi, M.-O., Kakitani, M., Yamashita, T., Tomizuka, K. and Hanaoka, K. (2009). Targeted deletion of the type IIb Na(+)-dependent Pi-co-transporter, NaPi-IIb, results in early embryonic lethality. *Biochem. Biophys. Res. Commun.* **381**, 482-486. doi:10.1016/j.bbrc.2009.02.067
- Shin, J., Bossenz, M., Chung, Y., Ma, H., Byron, M., Taniguchi-Ishigaki, N., Zhu, X., Jiao, B., Hall, L. L., Green, M. R. et al. (2010). Maternal Rnf12/RLIM is required for imprinted X-chromosome inactivation in mice. *Nature* **467**, 977-981. doi:10.1038/nature09457
- Simon, J. A. and Kingston, R. E. (2009). Mechanisms of polycomb gene silencing: knowns and unknowns. *Nat. Rev. Mol. Cell Biol.* **10**, 697-708. doi:10.1038/nrm2763
- Tam, P. P. L. (1988). Postimplantation development of mitomycin C-treated mouse blastocysts. *Teratology* **37**, 205-212. doi:10.1002/tera.1420370305
- Tam, P. P. L. and Loebl, D. A. F. (2007). Gene function in mouse embryogenesis: get set for gastrulation. *Nat. Rev. Genet.* **8**, 368-381. doi:10.1038/nrg2084
- Tanaka, S., Kunath, T., Hadjantonakis, A.-K., Nagy, A. and Rossant, J. (1998). Promotion of trophoblast stem cell proliferation by FGF4. *Science* **282**, 2072-2075. doi:10.1126/science.282.5396.2072
- Tanaka, S., Oda, M., Toyoshima, Y., Wakayama, T., Tanaka, M., Yoshida, N., Hattori, N., Ohgane, J., Yanagimachi, R. and Shiota, K. (2001). Placentomegaly

- in cloned mouse concepti caused by expansion of the spongiotrophoblast layer. *Biol. Reprod.* **65**, 1813-1821. doi:10.1095/biolreprod65.6.1813
- Walentin, K., Hinze, C. and Schmidt-Ott, K. M.** (2016). The basal chorionic trophoblast cell layer: An emerging coordinator of placenta development. *BioEssays* **38**, 254-265. doi:10.1002/bies.201500087
- Wang, L.-Y., Li, Z.-K., Wang, L.-B., Liu, C., Sun, X.-H., Feng, G.-H., Wang, J.-Q., Li, Y.-F., Qiao, L.-Y., Nie, H. et al.** (2020). Overcoming intrinsic H3K27me3 imprinting barriers improves post-implantation development after somatic cell nuclear transfer. *Cell Stem Cell* **27**, 315-325. doi:10.1016/j.stem.2020.05.014
- Xie, Z., Zhang, W. and Zhang, Y.** (2022). Loss of Slc38a4 imprinting is a major cause of mouse placenta hyperplasia in somatic cell nuclear transferred embryos at late gestation. *Cell Rep.* **38**, 110407. doi:10.1016/j.celrep.2022.110407
- Yan, J., Dutta, B., Hee, Y. T. and Chng, W.-J.** (2019). Towards understanding of PRC2 binding to RNA. *RNA Biol.* **16**, 176-184. doi:10.1080/15476286.2019.1565283
- Yu, J.-R., Lee, C.-H., Oksuz, O., Stafford, J. M. and Reinberg, D.** (2019). PRC2 is high maintenance. *Genes Dev.* **33**, 903-935. doi:10.1101/gad.325050.119
- Zenk, F., Loeser, E., Schiavo, R., Kilpert, F., Bogdanović, O. and Iovino, N.** (2017). Germ line-inherited H3K27me3 restricts enhancer function during maternal-to-zygotic transition. *Science* **357**, 212-216. doi:10.1126/science.aam5339
- Zhang, B., Zheng, H., Huang, B., Li, W., Xiang, Y., Peng, X., Ming, J., Wu, X., Zhang, Y., Xu, Q. et al.** (2016). Allelic reprogramming of the histone modification H3K4me3 in early mammalian development. *Nature* **537**, 553-557. doi:10.1038/nature19361
- Zheng, H., Huang, B., Zhang, B., Xiang, Y., Du, Z., Xu, Q., Li, Y., Wang, Q., Ma, J., Peng, X. et al.** (2016). Resetting epigenetic memory by reprogramming of histone modifications in mammals. *Mol. Cell* **63**, 1066-1079. doi:10.1016/j.molcel.2016.08.032
- Zhu, M. and Zernicka-Goetz, M.** (2020). Principles of self-organization of the mammalian embryo. *Cell* **183**, 1467-1478. doi:10.1016/j.cell.2020.11.003

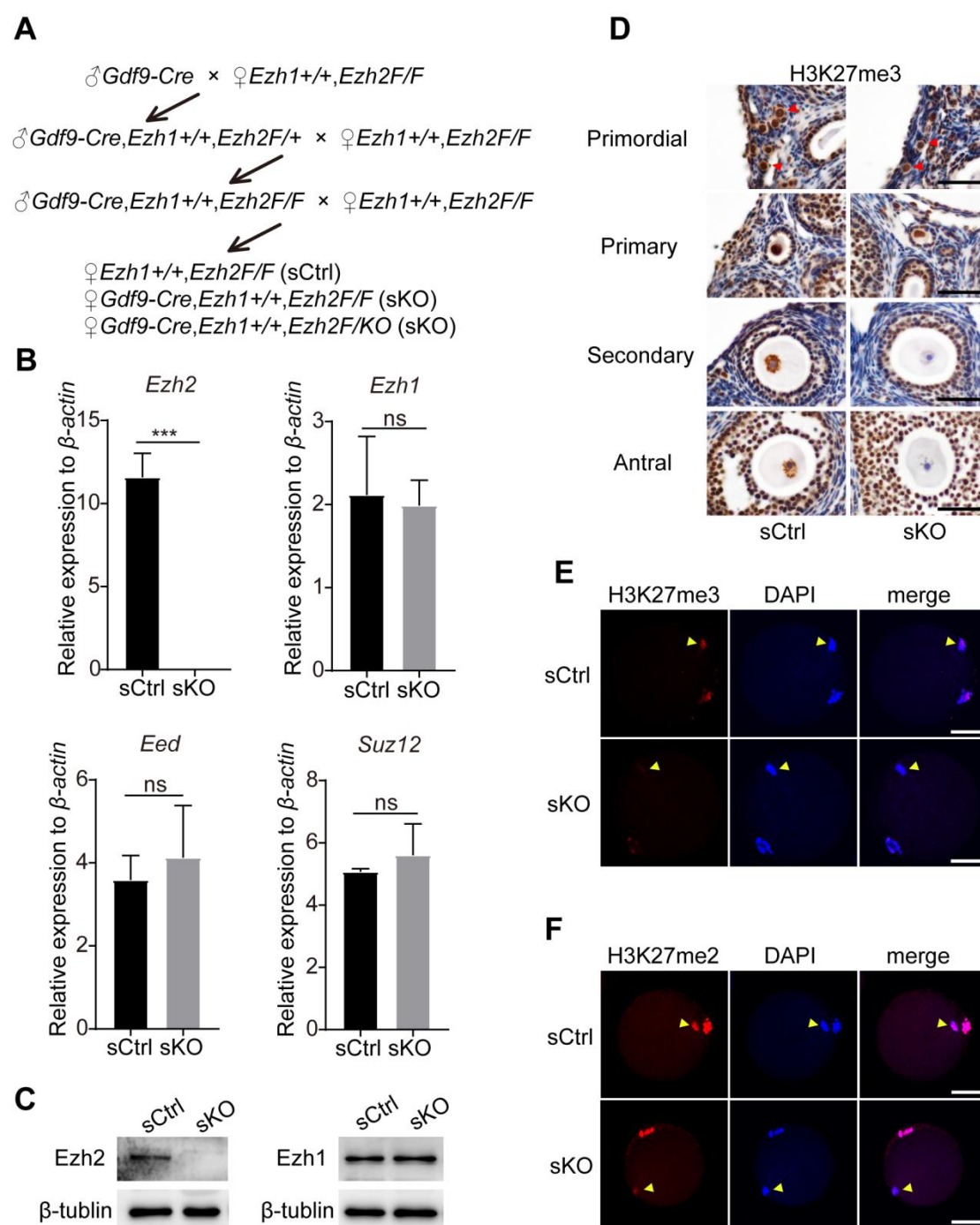


Fig. S1. Generation of maternal *Ezh2* deficient mice and knockout efficiency in oocytes. (A) Breeding scheme used to generate sCtrl and sKO mice. (B) Real-time PCR analysis of mRNA level for *Ezh2*, *Ezh1*, *Eed* and *Suz12* in sCtrl and sKO oocytes. Data are presented as the mean \pm SD. Unpaired *t* test: ns, not significant; ****P* < 0.001. (C) Levels of *Ezh2* and *Ezh1* protein in oocytes as assessed by western blot analysis; β -tubulin was used as loading control. (D) H3K27me3 in

oocytes from primordial, primary, secondary and antral follicles checked by immunohistochemical (IHC) staining. Ovary sections were stained with anti-H3K27me3 antibody and counterstained with hematoxylin. The primordial follicles were indicated by red arrows. Scale bars, 50 μ m. **(E and F)** H3K27me3 and H3K27me2 in super-ovulated oocytes measured by immunofluorescence (IF) staining. The chromosomes of oocytes were indicated by yellow arrows. Number of oocytes examined for H3K27me3: sCtrl, n=27; sKO, n=21. For H3K27me2: sCtrl, n=16; sKO, n=20. Scale bars, 50 μ m.

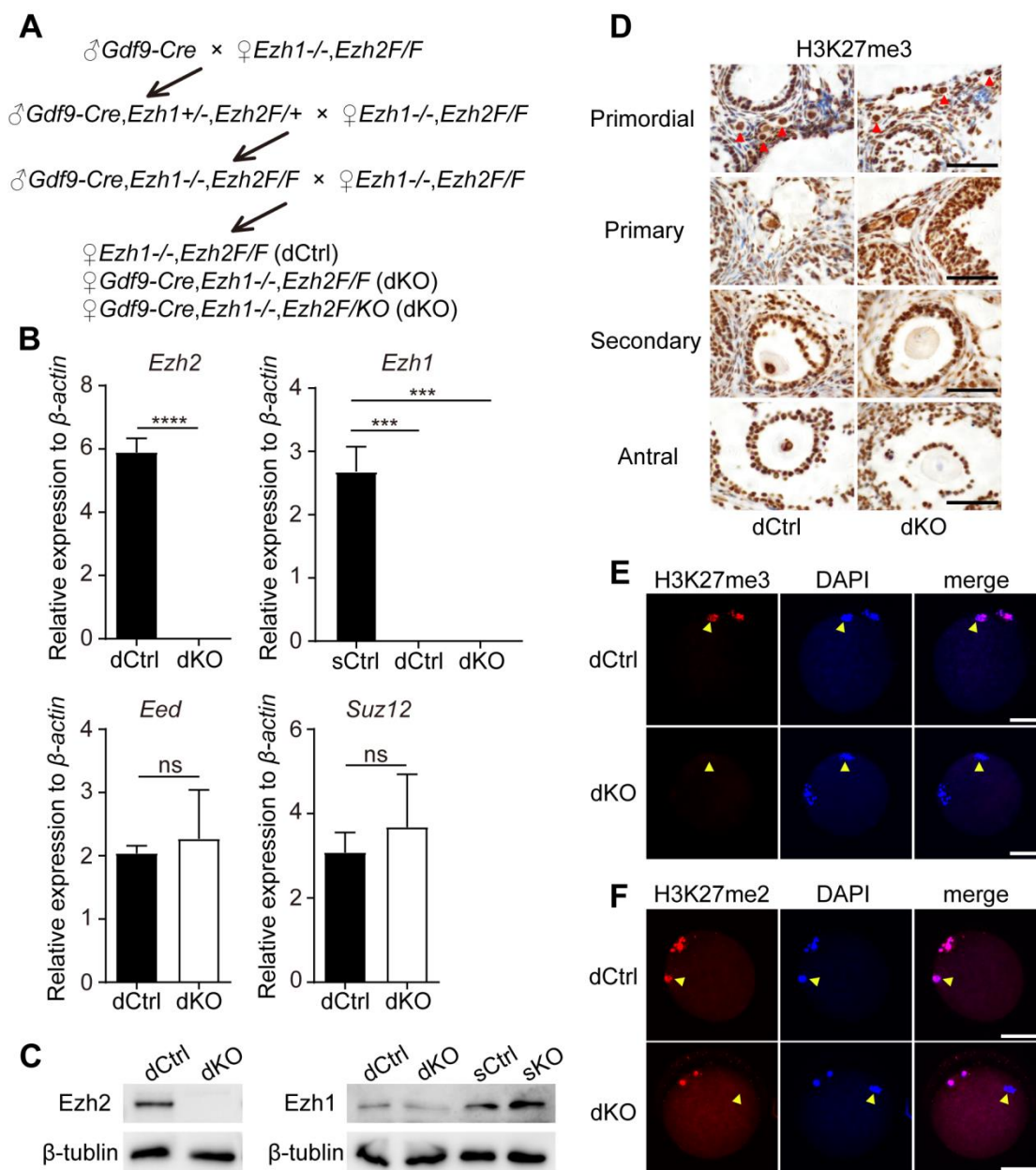


Fig. S2. Generation of maternal *Ezh1/2* deficient mice and knock out efficiency in oocytes. (A) Breeding scheme used to generate dCtrl and dKO mice. (B) Real-time PCR analysis of *Ezh2*, *Ezh1*, *Eed* and *Suz12* transcripts in dCtrl and dKO oocytes. Data are presented as the mean \pm SD. Unpaired *t* test: ns, not significant; ****P* < 0.001; *****P* < 0.0001. (C) Levels of *Ezh2* and *Ezh1* protein in oocytes as assessed by western blot analysis; β -tubulin was used as loading control. (D) IHC staining showed H3K27me3 modification in oocytes from primordial, primary, secondary and antral follicles. Ovary sections were stained with anti-H3K27me3 antibody and then counterstained with hematoxylin. The primordial follicles were indicated by red arrows. Scale bars, 50 μ m. (E and F) IF analysis of H3K27me3 and H3K27me2 in super-ovulated oocytes. The chromosomes of oocytes were indicated by yellow arrows. Number of oocytes examined for H3K27me3: dCtrl, n=16; dKO, n=28. For H3K27me2: dCtrl, n=24; dKO, n=32. Scale bars, 50 μ m.

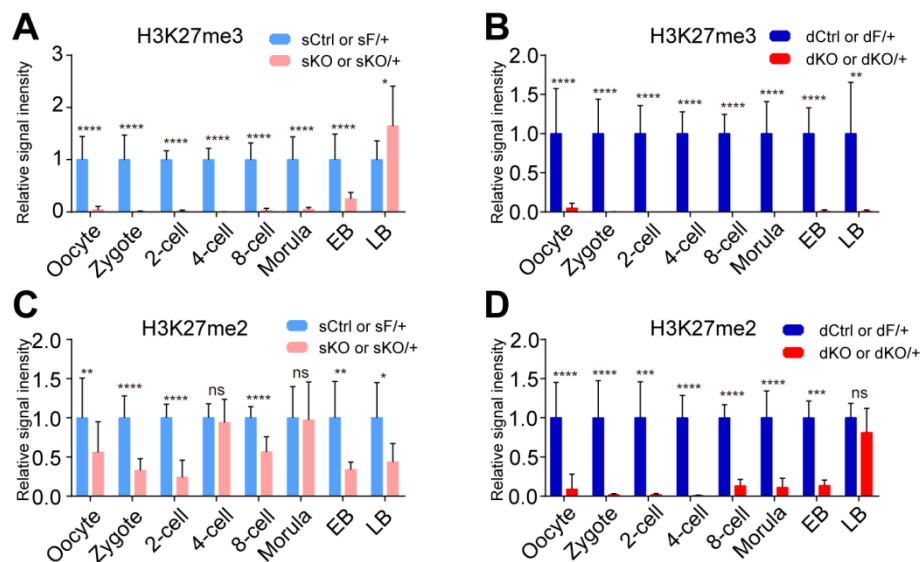


Fig. S3. The relative level of H3K27me3 and H3K27me2 signals in oocytes and embryos. (A) Relative H3K27me3 signal intensity in single knockout groups. (B) Relative H3K27me3 signal intensity in double knockout groups. (C) Relative H3K27me2 signal intensity in single knockout groups. (D) Relative H3K27me2 signal intensity in double knockout groups. EB, early blastocyst; LB, late blastocyst. The average signals of control oocytes or embryos were set as 1.0. Results are presented as mean \pm SD. Mann Whitney test or unpaired t test: ns, not significant; * $P < 0.05$; ** $P < 0.01$; *** $P < 0.001$; **** $P < 0.0001$.

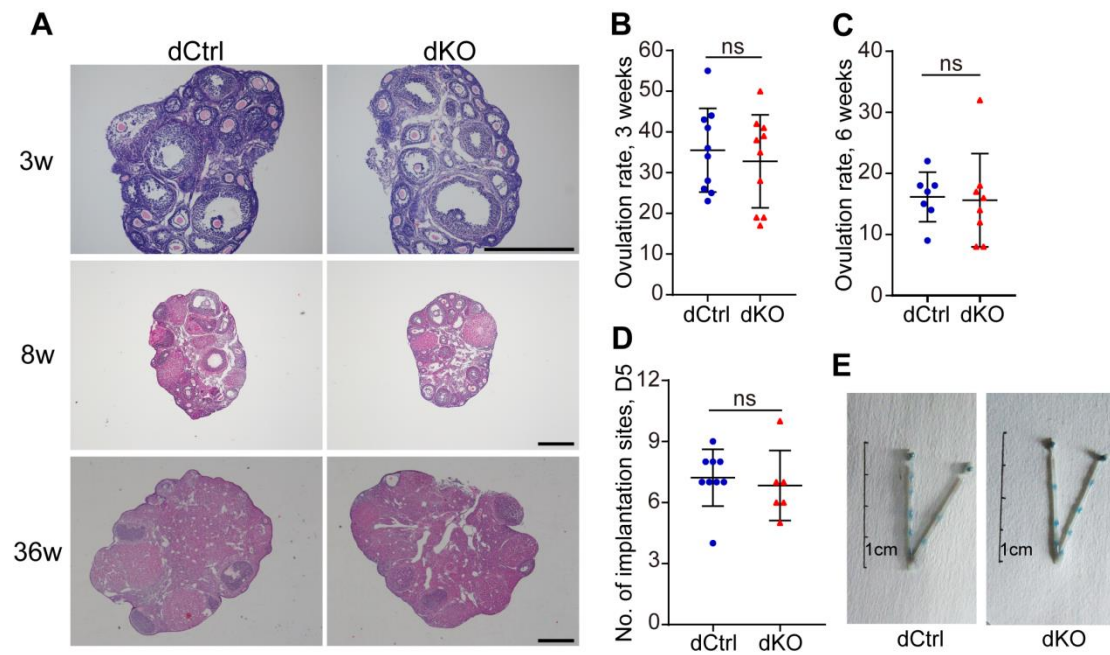


Fig. S4. Ovary morphology, ovulation rate and implantation site in dCtrl and dKO female mice. (A) Ovary sections stained with hematoxylin-rosin (HE) from 3-, 8-, and 36-wk-old mice. 3-wk-old mice were treated with PMSG for 46 hours. Scale bars, 500 μ m. (B and C) The number of ovulated oocytes per female mouse with superovulation treatment. (D) The number of implantation sites on Day 5 of pregnancy in dCtrl and dKO mice. (E) Representative images of uteri with implantation sites on Day 5. Scale bars, 1cm. Results are presented as mean \pm SD. Statistical comparisons of values were made using unpaired *t* test (B and C) or Mann Whitney test (D). ns, not significant.

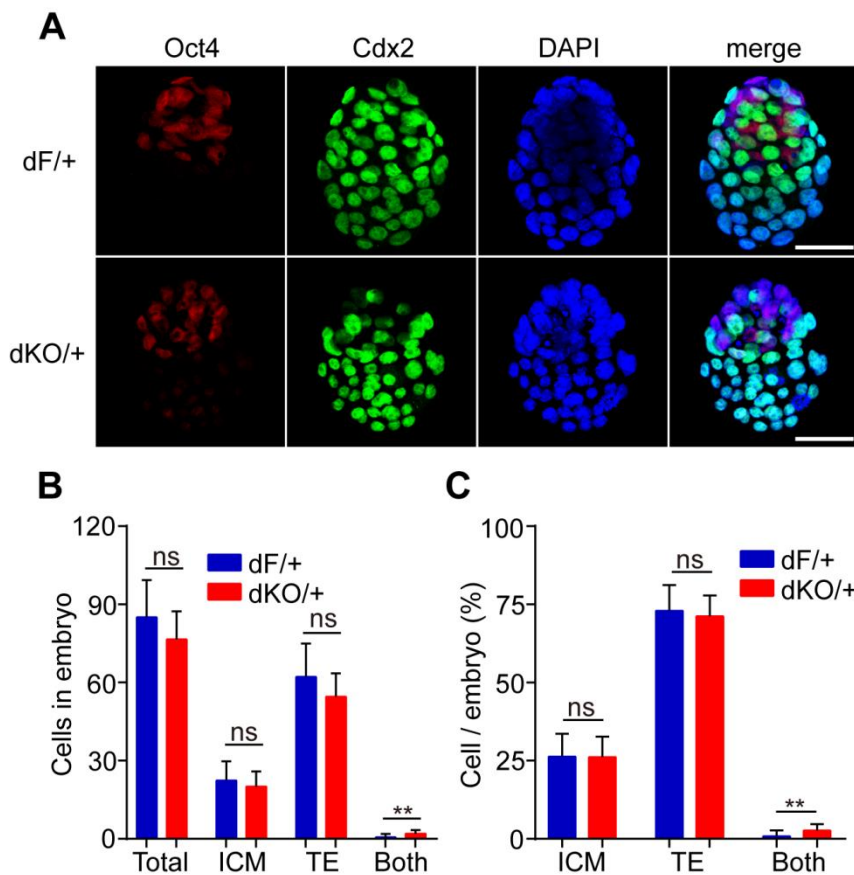


Fig. S5. The normal differentiation of trophoblast (TE) and the inner cell mass (ICM) in dKO/+ embryos at E3.75. (A) Representative images of Oct4 and Cdx2 immunostaining in embryos at E3.75. Inner cell mass (ICM) were stained with Oct4 (red) and trophoblast (TE) cells were stained with Cdx2 (green). Number of total embryos: dF/+, n=13; dKO/+, n=11. Scale bars, 50 μ m. (B) The number of different cell parts in embryos at E3.75. Results are presented as mean \pm SD. Statistical comparisons of values were made using Mann Whitney test (Total and Both) or unpaired *t* test (ICM and TE). ns, not significant; ***P* < 0.01. (C) The proportion of different cell parts at E3.75. Both: mix-expression of Oct4 and Cdx2. Results are presented as mean \pm SD. Statistical comparisons of values were made using Mann Whitney test (Both) or unpaired *t* test (ICM and TE). ns, not significant; ***P* < 0.01.

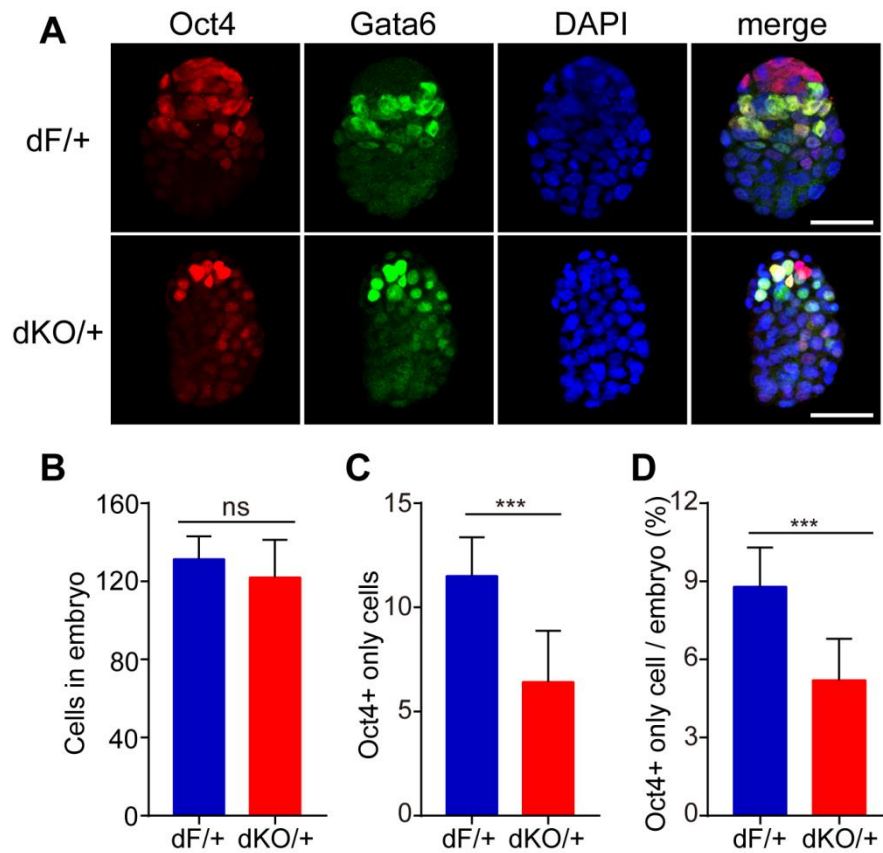


Fig. S6. Oct4⁺ only cells were decreased at E4.5. (A) Representative images of Oct4 and Gata6 in embryos at E4.5. ICM cells were labeled by Oct4 (red) and PrE cells were marked by Gata6 (green). Number of total embryos: dF/+, n=6; dKO/+, n=19. Scale bars, 50 μ m. (B) The average number of total cells in embryos. Results are presented as mean \pm SD. Mann Whitney test: ns, not significant. (C) Decreased Oct4⁺ only cells in dKO/+ embryos. Results are presented as mean \pm SD. Mann Whitney test: *** P < 0.001. (D) Ratio of EPI cells classified by Oct4⁺ only cells. Results are presented as mean \pm SD. Mann Whitney test: *** P < 0.001.

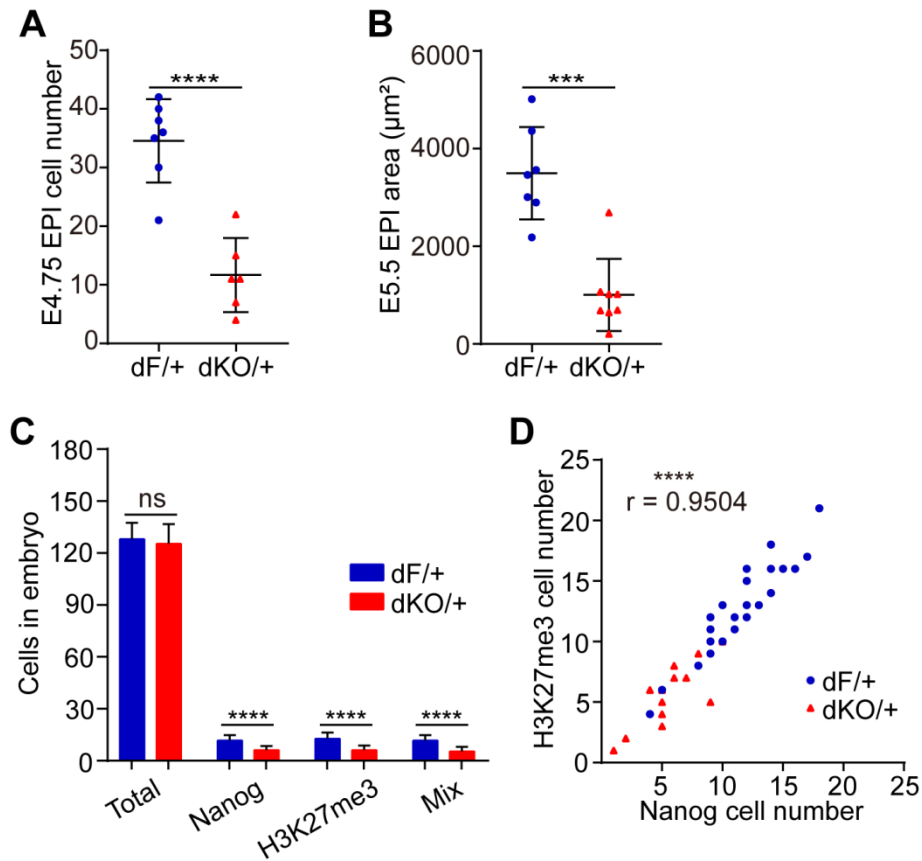


Fig. S7. Decreased EPI cells from E4.5 to E5.5. (A) EPI cell number at E4.75. Number of total embryos: dF/+, n=7; dKO/+, n=6. Results are presented as mean \pm SD. Unpaired *t* test: *****P* < 0.0001. **(B)** EPI area at E5.5. Results are presented as mean \pm SD. Mann Whitney test: ****P* < 0.001. **(C)** Decreased Nanog and H3K27me3 cells in dKO/+ embryos. Mix: cells showed both Nanog and H3K27me3 staining. Results are presented as mean \pm SD. Unpaired *t* test: ns, not significant; *****P* < 0.0001. **(D)** Correlation analysis of Nanog and H3K27me3 cell numbers. Number of total embryos: dF/+, n=31; dKO/+, n=17. The cell numbers is highly correlated; Pearson *r* = 0.9504. *****P* < 0.0001.

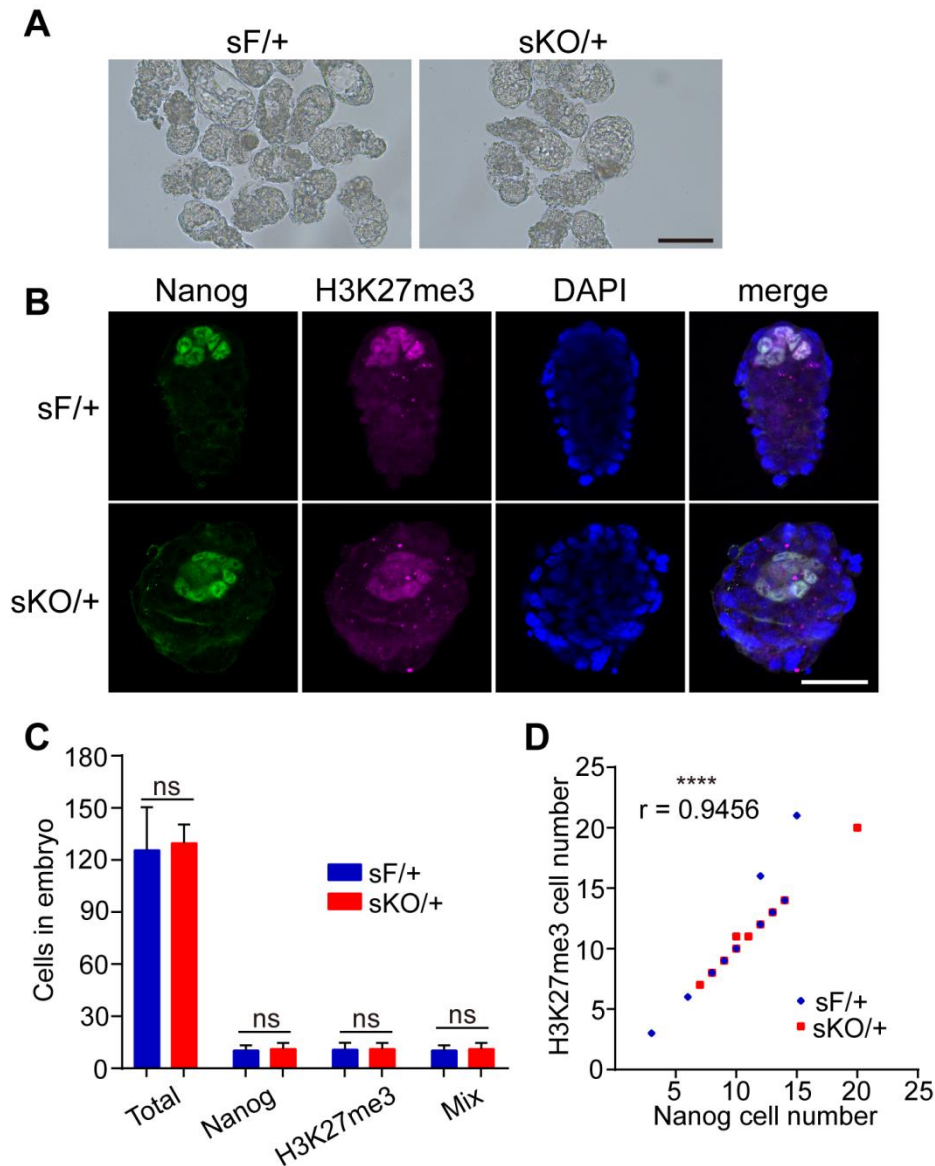


Fig. S8. Normal epiblast cells in sKO/+ Embryos at E4.5. (A) Representative images of flushed embryos at E4.5. Scale bars, 100 μ m. (B) Representative images of late blastocysts immunostained with Nanog and H3K27me3. Number of total embryos: sF/+, n=31; sKO/+, n=35. Scale bars, 50 μ m. (C) Quantitative analysis of Nanog and H3K27me3 cells. Mix: cells showed both Nanog and H3K27me3 staining. Results are presented as mean \pm SD. Mann Whitney test: ns, not significant. (D) Correlation analysis of Nanog and H3K27me3 cell numbers. Number of total embryos: sF/+, n=31; sKO/+, n=35. The cell numbers is highly correlated; Pearson $r = 0.9456$. **** $P < 0.0001$.

Table S1. Embryo transfer

Group	No. of recipients	No. of blastocysts transferred	Pups per litter	Term pups (%)
dF/+	13	170	6.31 ± 2.32	82 (48.24%)
dKO/+	9	111	2.22 ± 1.86***	20 (18.02%****)

Pups per recipient are recorded as mean ± SD. Statistical comparisons were made using Mann Whitney test, *** $P < 0.001$. Comparisons between dF/+ and dKO/+ about Pups (%) were by χ^2 test, **** $P < 0.0001$.

Table S2. Primers

Gene	Sequence (5' to 3')	Reference
Primers for genotype		
<i>Ezh2</i> -F	GCTAGAAGCATTCCCCACAC	
<i>Ezh2</i> -R	CTGGCTCTGTGGAACCAAAC	
<i>Ezh2</i> -R (within <i>lacZ</i>)	ATGGGCCTCATAGTGACAGG	
<i>Ezh1</i> -F	GATGCCCTCAACCAGTACTC	
<i>Ezh1</i> -R	TTTATATCACGCACCCACAC	
<i>Ezh1</i> -R (within <i>lacZ</i>)	TAAAGCGAGTGGCAACATGG	
<i>Gdf9</i> -Cre-F	TCTGATGAAGTCAGGAAGAACC	
<i>Gdf9</i> -Cre-R	GAGATGTCCTTCACTCTGATTC	
Internal control-F	CAAATGTTGCTTGTCTGGTG	
Internal control-R	GTCAGTCGAGTGCACAGTTT	
Primers for real-time PCR		
<i>Ezh2</i> -F	TGACCCTGACCTCTGTCTCACG	
<i>Ezh2</i> -R	TCAGACGGTGCCAGCAGTAAGT	
<i>Ezh1</i> -F	AGCGATGCTGTGTTTCTGGA	
<i>Ezh1</i> -R	GGCGCTTCCGTTTCTTGTT	
<i>Eed</i> -F	ATGCCATTGTATGCTGGAAACC	
<i>Eed</i> -R	CACTGGCTGTAATCAAATCGCC	
<i>Suz12</i> -F	TCTCATCGAAATTCCAGAACAAGC	
<i>Suz12</i> -R	CAAGCTATGAGATTCTTGCTCTCC	
β -actin-F	GTGACGAGGCCCAAGCAAGAG	(1)
β -actin-R	CGTACATGGCTGGGGTGTTGAAGG	

Table S3. Antibodies

Antibody	Source	Concentration
Rabbit polyclonal Anti-Ezh2	Abcam, ab186006	WB: 1:500
Mouse monoclonal Anti-beta tubulin	Proteintech, 66240	WB: 1:2000
Rabbit monoclonal Anti-H3K27me3	CST, 9733	IHC: 1:2500 IF: 1:400
Rabbit monoclonal Anti-Vcam1	Abcam, ab134047	IHC: 1:1000
Rabbit polyclonal Anti-integrin alpha 4	Santa Cruz, sc14008	IHC: 1:1000
Rabbit monoclonal Anti-H3K27me2	CST, 9728	IF: 1:400
Rabbit monoclonal Anti-Oct4	Abcam, ab200834	IF: 1:200
Mouse monoclonal Anti-Cdx2	Biogenex, CDX-88	IF: 1:200
Rabbit polyclonal Anti-Nanog	Abcam, ab80892	IF: 1:200
Goat polyclonal Anti-Gata6	R&D systems, AF1700	IF: 1:200
Alexa Fluor 594 Goat Anti-Rabbit IgG	ZSBIO, ZF-0516	IF: 1:200
Alexa Fluor 488 Goat Anti-Mouse IgG	ZSBIO, ZF-0516	IF: 1:200
Alexa Fluor 568 Donkey Anti-Rabbit IgG (H+L)	Abcam, ab175693	IF: 1:500
Alexa Fluor 594 Donkey Anti-Rabbit IgG (H+L)	YEASEN, 34212ES60	IF: 1:200
Alexa Fluor 488 Donkey Anti-Goat IgG (H+L)	YEASEN, 34306ES60	IF: 1:200
Alexa Fluor 647 Donkey Anti-Mouse IgG (H+L)	YEASEN, 34113ES60	IF: 1:200

Table S4. Putative H3K27me3-dependent imprinted genes

[Click here to download Table S4](#)

Reference

1. Ciccone DN, Su H, Hevi S, Gay F, Lei H, Bajko J, et al. KDM1B is a histone H3K4 demethylase required to establish maternal genomic imprints. *Nature*. 2009;461(7262):415-8.